Washington University in St. Louis
Washington University Open Scholarship

McKelvey School of Engineering Theses & Dissertations | McKelvey School of Engineering

Winter 12-15-2015

Optimization of Looped Airfoil Wind Turbine (LAWT) and Looped Airfoil Hydro-Turbine (LAHT) Design Parameters for Maximum Power Generation

Binhe Song
Washington University in St Louis

Follow this and additional works at: https://openscholarship.wustl.edu/eng_etds

 Part of the Engineering Commons

Recommended Citation

Song, Binhe, "Optimization of Looped Airfoil Wind Turbine (LAWT) and Looped Airfoil Hydro-Turbine (LAHT) Design Parameters for Maximum Power Generation" (2015). *McKelvey School of Engineering Theses & Dissertations*. 124.
https://openscholarship.wustl.edu/eng_etds/124

This Thesis is brought to you for free and open access by the McKelvey School of Engineering at Washington University Open Scholarship. It has been accepted for inclusion in McKelvey School of Engineering Theses & Dissertations by an authorized administrator of Washington University Open Scholarship. For more information, please contact digital@wumail.wustl.edu.

WASHINGTON UNIVERSITY IN ST. LOUIS

School of Engineering and Applied Science

Department of Mechanical Engineering and Material Science

Thesis Examination Committee:
Ramesh K. Agarwal, Chair
David A. Peters
Kenneth Jerina

Optimization of Looped Airfoil Wind Turbine (LAWT) and Looped Airfoil Hydro-Turbine (LAHT) Design Parameters for Maximum Power Generation

by

Binhe Song

A thesis presented to the School of Engineering & Applied Science
of Washington University in St. Louis in partial fulfillment of the
requirements for the degree of
Master of Science

December 2015

Saint Louis, Missouri

© 2015, Binhe Song

Contents

List of Figures

List of Tables

Acknowledgments

First of all, I would like to express my sincere gratitude to my advisor Prof. Ramesh Agarwal for his continuous support of my academic study and related research, for his patience, motivation, and immense knowledge. His guidance helped me enormously in this research and in writing of this thesis. I am so honored to be his student.

Besides my advisor, I would like to thank the rest of my thesis committee, Prof. Peters and Prof. Jerina, for their insightful comments and encouragement.

My sincere thanks also go to Tim Wray and Xu Han for providing technical advice whenever I needed it.

Last but not least, I especially want to thank Subhodeep Banerjee for developing analytical equation of power generation from LAWT/LAHT and for his continued guidance throughout this research.

Binhe Song

Washington University in St. Louis
December 2015

Dedicated to my beloved parents, Yahui Wang and Guojun Song.

ABSTRACT

Optimization of Looped Airfoil Wind Turbine (LAWT) and Floating Looped Airfoil Hydro-Turbine (LAHT) Design Parameters for Maximum Power Generation

by

Binhe Song

Master of Science in Mechanical Engineering

Washington University in St. Louis, 2015

Research Advisor: Professor Ramesh K. Agarwal

This focus of this research is on the study of the aerodynamic performance of a Looped Airfoil Wind Turbine (LAWT™) using the Computational Fluid Dynamics (CFD) software. The looped airfoil wind turbine (LAWT™) is a patented new technology by EverLift Wind Technology, Inc. for generating power from wind. It takes advantage of the superior lift force of a linearly traveling wing compared to the rotating blades in conventional wind turbine configurations. Compared to horizontal and vertical axis wind turbines, the LAWT™ can be manufactured with minimal cost because it does not require complex gear systems and its blades have a constant profile along their length. These considerations make the LAWT™ economically attractive for small-scale decentralized power generation in rural areas. Each LAWT™ is estimated to generate power in the range of 10 kW to 1 MW. Due to various advantages, it is meaningful to determine the maximum possible power generation of a LAWT™ by optimizing its structural layout.

In this study, CFD simulations were conducted using ANSYS Fluent to determine the total lift and drag coefficient of a cascade of airfoils. The adaptive structured meshes were created using the commercial mesh generating software ICEM. The k-kl-ω turbulence model was used to account for flow in the laminar-turbulent transition region. Given the lift and drag coefficients and the kinematics of the system, an analytical formula for the power generation of the LAWT™ was developed. General formulas were obtained for the average lift and drag coefficients so that the total power could be predicted for any number of airfoils in LAWT™. The spacing between airfoils and the track angle were identified as the key design parameter that affected the power generation of the

LAWT™. The results showed that a marked increase in total power could be achieved if the optimum spacing between the airfoils was used for a given track angle. The same idea was then applied to study an analogous floating Looped Airfoil Hydro-Turbine (LAHT) which converts the kinetic energy of river streams into electricity. The results showed that each LAHT of the same configuration as LAWT can generate nearly 756% more power than the power generated by the LAWT due to much higher density of water compared to air. Finally, to generate more power from LAWT and LAHT, a new highly-cambered airfoil was studied to generate more lift and drag to generate more power. Thus various parameters of LAWT and LAHT were optimized for generating optimum power.

Chapter 1 Introduction

1.1 Background

Wind turbine is a device that converts kinetic energy from the wind into electrical power. There are mainly two types of wind turbines: the horizontal-axis wind turbine (HAWT) and the vertical-axis wind turbine (VAWT), which rotate about a horizontal and a vertical axis respectively. Wind turbine design involves the methodology of defining the form and specifications of a wind turbine to extract energy from the wind [1]. The design of HAWT blades employs the concept used in the design of helicopter blades. Recently, a novel wind turbine concept (Looped Airfoil Wind Turbine) has been invented by George Syrovy and his team at EverLift Inc. Looped Airfoil Wind Turbine (LAWT) consists of a basic system of a triangular structure utilizing both lift and drag aerodynamic forces produced by the wind [3]. Conventional wind turbine such as HAWT uses the "rotary wing" concept of a helicopter, whereas the LAWT uses the "fixed-wing" concept of an airplane.

The idea of LAWT came about when EverLift cofounder George Syrovy invented a novel vertical takeoff and landing aircraft that involved extensive investigation of helicopter rotors, basically the rotating wings. Syrovy noticed that the horizontal wind turbine rotors have helicopter-like blades embodying all the limitations of the rotary wing aircraft. This insight led to the idea of capturing wind energy using multiple airfoils in the manner of a fixed-wing aircraft. The LAWT design appears to work equally well in both wind and flowing water [4].

The concept of LAWT was first demonstrated in the Wind Power 2013 exhibition. It is supposed to overcome the shortcomings of the horizontal wind turbines. From Fig.1.1 it can be seen that this device looks like a conveyor belt with airfoils for cleats. The airfoils travel across the wind and then push the belt along the track due to generation of lift and drag. The moving chain via a rack-and-pinion setup can drive the electric generators. The inventor mentions that one advantage of LAWT is that wing on both ascending and descending tracks capture the wind energy and the LAWT concept works equally well in both air and water. Thus the LAWT concept can also be turned into a floating Looped Airfoil Hydro-Turbine (LAHT) that can harvest energy from river streams which is also abundant and renewable. Also, in comparison to the conventional horizontal wind turbines, the heavy parts of LAWT are at the ground level.

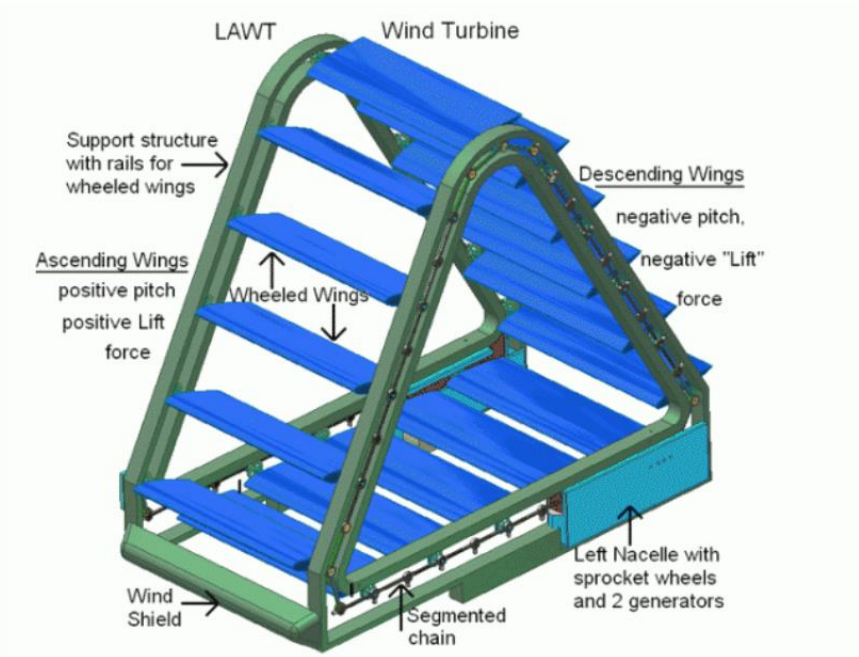

Figure 1.1: Schematic of a Looped Airfoil Wind Turbine (LAWT)

1.2 Motivation

Conventional wind turbines such as HAWT are very heavy and tall, sometimes they weigh as much as 250 tons at a height of 150 meters. Hence they require heavy reduction gears and are failure-prone to yaw control and pitch control. LAWT is much smaller and can share a single raft or barge platform which HAWT cannot do. The blades of HAWT are also complex and expensive to manufacture, transport and install. Since conventional wind turbines such as HAWT use the "rotary wing" concept of a helicopter, the blades of HAWT act like helicopter rotor blades that lead to inefficiencies. George Syrovy's work on helicopters led him to an awareness of such weaknesses of conventional wind turbines. He therefore concluded that the fixed-wing type looping airfoil wind turbine is likely to have better efficiency and much cheaper.

The fixed-wing airfoils in LAWT can move linearly. The airfoils are linked together on a triangular track as shown in Fig. 1.1, and the system incorporates a power extraction mechanism. LAWT takes advantage of the superior lift force of a linearly traveling wing compared to the lift and drag generated on rotating blades in conventional wind turbine configurations [2]. Looped Airfoil Wind Turbine has other advantages, it does not require complex gear systems and its blades have a

constant profile along their length and therefore LAWT can be manufactured at much lower cost than a comparable HAWT for the same amount of power. Furthermore, by placing the yaw rotation center (the center of rotation of the base around a vertical axis) ahead of the center of the triangular structure, LAWT automatically orients itself such that the wings on the ascending track face the wind. It also eliminates the need to lock the yaw position of the device as required by a conventional wind turbine [3]. Furthermore, several LAWTs can be placed much closer to each whereas conventional wind turbines such as HAWT require a minimum distance from each other (usually 5 to7 times its rotor diameter). Additionally, the LAWT concentrates its weight at the base of the triangular structure, and does not require tall and anchored pylons. Since it sits on an offset rotating baseplate, the LAWT does not require sophisticated yaw control, either for power regulation or to prevent overspeeding [5]. Also, the LAWT does not require complex, expensive and maintenance-intensive pitch control since all blades have a constant angle of attack. Another design feature of LAWT is that its airfoils can extract wind's energy on both the ascending and descending track. Thus, the prospects of LAWT for small and medium range wind power generation of the order of 10 KW to 1 MW look promising.

The concept of a LAWT has never been evaluated theoretically and numerically in the literature before. The goal of this thesis is to perform numerical simulation and compute the power generated by a LAWT and then compare it with experimentally available information for a model LAWT [3]. Another goal is to optimize various design parameters of the LAWT, namely the track angle and the distance between the airfoils to maximize the power generation. The final objective is to extend the concept of LAWT to LAHT and analyze and optimize the performance of a LAHT by numerical simulation using CFD technology.

Chapter 2 Modeling and Analysis Tools

2.1 Mesh Generation Software-ANSYS ICEM

ANSYS ICEM is a popular proprietary software package used for mesh generation. It can create structured, unstructured, multi-block, and hybrid grids with different cell geometries. ANSYS ICEM provides advanced geometry acquisition, mesh generation, and mesh optimization to meet the requirement for integrated mesh generation and post processing tools for sophisticated analysis of complex configuration. ANSYS ICEM is used in conjunction with flow modeling software such as ANSYS FLUENT to solve engineering problems involving fluid flow.

ANSYS ICEM can be considered as an extension of the meshing capabilities of original ANSYS meshing software. ICEM can be used outside of the workbench to mesh from faceted geometry and is easy to use and fits into the workbench.

In this thesis, all geometry modelling was created using ANSYS ICEM. After geometry modelling, the unstructured meshes were created which were then imported into ANSYS FLUENT for fluid flow simulations.

2.2 CFD Flow Solver-ANSYS FLUENT

ANSYS FLUENT is a Computational Fluid Dynamics (CFD) tool for simulating fluid flows in a virtual environment used by engineers for design and analysis of many industrial products. It is owned by ANSYS, Inc. Capabilities of FLUENT include modeling of fluid including the effects of flow, turbulence, heat transfer, and chemical reactions. FLUENT is currently extensively employed in both industry and academic research.

In this thesis, all fluid field simulations were conducted using ANSYS FLUENT.

Chapter 3 Flow Field Simulations of Cascade of NACA 64421 Airfoils and Optimization Methodology for Looped Airfoil Wind Turbine

LAWT utilizes aerodynamics forces generated by wind for power generation. The LAWT takes advantage of the superior aerodynamic performance of an airplane wing compared to conventional wind turbines with rotating blades [3]. The wings in a LAWT are mounted on a trapezoidal track and are connected by chains. The wings are evenly spaced on a triangular structure with their leading edges parallel, traveling up and down in a triangular path. The entire system moves together due to aerodynamic forces on the wings in the ascending and descending portions of the track [3]. When the wings are powered by the positive lift force, they travel upward in the clockwise direction. The airfoils are connected to each other by a chain. The chain can transfer kinetic mechanical power to electric generators. The rotor blades in conventional wind turbines are very complex and expensive to design and manufacture. However, as can be seen from Fig. 1.1, a LAWT utilizes planar wings with uniform airfoil section instead of the traditional three long rotating blades used in a HAWT. Since each wing on the track has a uniform airfoil section along its length, it can significantly reduce the manufacturing cost. Furthermore the LAWT design is flexible, it can be adjusted to face the wind direction all the time or can stay in a fixed position.

The wing sections in a LAWT can be either symmetrically or asymmetrically having a camber. The ascending wings can be positioned at an angle of attack ranging from 0 to 18 degrees. The LAWT structure has three tracks: an ascending track at an angle, a descending track at an angle and a horizontal bottom track. The optimal track angle is 60 degrees; it can vary between 45 to 75 degrees. To find the optimal LAWT configuration to maximize the power generation, several design parameters must be considered, such as the spacing between the wings, the track speed, and the angle of the ascending and descending tracks. This thesis develops an analytical expression for the power generated by the LAWT by calculating the average lift and drag coefficients for each wing based on the kinematics of the LAWT system. To calculate the average lift and drag coefficients,

numerical simulations for a cascade of airfoils on ascending and descending track are performed using ANSYS FLUENT. The simulation is also considered the effect of the ascending track angle and the spacing between the wings in order to determine the optimal parameters for maximum power generation.

3.1 Kinematics of a Wing with Constant Airfoil Section on Ascending Track

The LAWT is set in motion by the components of the lift and drag forces on wings in the direction of the ascending track. During start-up operation, the only velocity component seen by the airfoil is the wind (assumed horizontal). As a result, the high initial pitching angle also acts as the angle of attack and motion along the track is initiated primarily by the drag. As the track attains speed, the track motion induces a downwards velocity on the airfoil, which reduces the angle of attack seen by the airfoil, bringing the airfoil to a more favorable operating condition where the lift starts to contribute more to the resultant force along the track than the drag. Steady-state operation is reached when the track reaches its design speed and brakes engage to prevent it from accelerating further.

The wings move along a track at an angle β to the horizontal. For a given wind speed U_W and a given track speed $U_T = fU_W$ (as a fraction of the wind speed, f<1). There are primarily three possible scenarios that can occur as illustrated in Fig 3.1. It is assumed that the track angle β is 60 degrees. Note that in each case, the angle of attack α remains at 12 degrees. The wind direction is at an angle φ with the horizontal direction. Now, the freestream velocity seen by the airfoils on the ascending track can be determined from the wind speed, the forward track angle, and the track speed using the cosine rule as shown in Eq. 3.1.

$$U_\infty^2 = U_W^2 + U_T^2 - 2U_W U_T \cos\beta \tag{3.1}$$

For the three cases with different track speed, the freestream velocity U_∞ is given in Table 3.1.

Table 3.1: Freestream Velocities for Different Track Speeds

	Case 1	Case 2	Case 3
Track Speed U_T	0.25 U_W	0.5 U_W	U_W
Freestream velocity U_∞	0.90 U_W	0.87 U_W	U_W

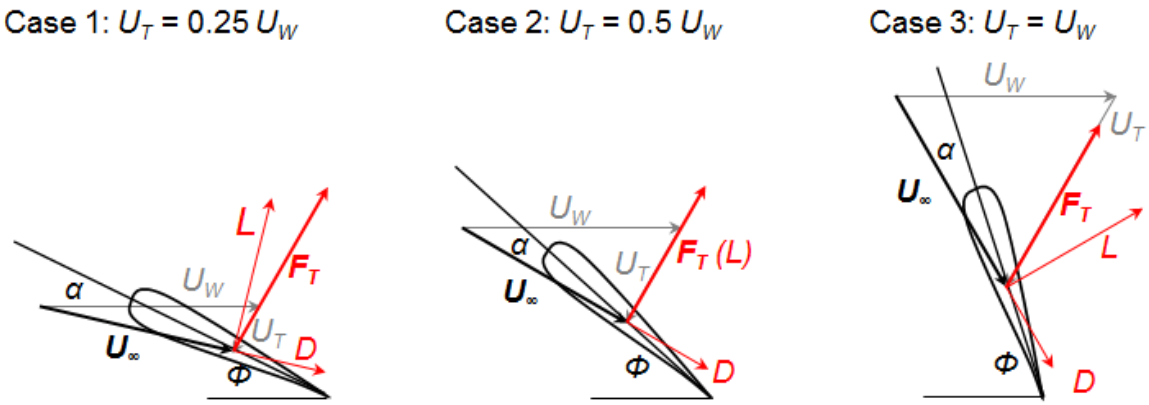

Figure 3.1: Freestream Velocities for Different Track Speeds

To maximize the wind speed, the design track speed in this study is considered to be equal to the wind speed, as shown in Fig. 3.2

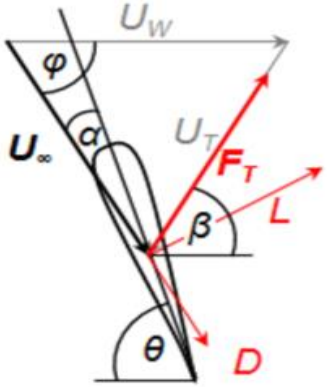

Figure 3.2: Kinematics of LAWT Airfoil on Ascending Track with Track Speed Equal to the Wind Speed

3.1.1 Kinematics of the LAWT Wings on Ascending Track

The freestream velocity seen by the airfoils on the ascending track can be found from the wind speed, the forward track angle, and the track speed using the cosine rule as given in Eq. 3.1. The freestream velocity given by Eq. 3.2 acts at an angle of φ from the horizontal.

$$\varphi = \text{acos}\left(\frac{U_\infty^2 + U_W^2 - U_T^2}{2U_\infty U_W}\right) \tag{3.2}$$

To ensure that the angle of attack seen by the airfoil during steady-state operation is the design angle of attack α, the airfoil must be pitched on the track at an angle θ with respect to the horizontal where $\theta = \alpha + \varphi$.

The lift and drag on the airfoil act perpendicular and parallel to the direction of the freestream respectively. The resultant force along the track as a result of the lift and drag is what powers the track motion. Assuming that the lift L and drag D are known, the net force along the track F_T can be computed from Eq. 3.3.

$$F_T = L\sin(\beta + \varphi) + D\cos(\beta + \varphi) \tag{3.3}$$

The one-dimensional resultant force coefficient along the track can be obtained from the airfoil lift and drag coefficients as given in Eq. 3.4.

$$C_F = C_L\sin(\beta + \varphi) + C_D\cos(\beta + \varphi) \tag{3.4}$$

3.1.2 Analytical Derivation of Power Generation from LAWT

As can be seen from Fig. 3.2, for the case when the track speed is equal to the wind speed, the direction of the drag is such that the contribution of the drag to the resultant force along the track is negative. However, since the lift is much greater than the drag during steady-state operation, the net force along the track remains positive to power the track motion.

For a single airfoil, the coefficients of lift and drag can be obtained from the literature. For cascade of airfoils in a LAWT configuration, differences from single airfoil values are expected due finite spacing between the airfoils. Numerical simulations are used to determine the average lift and drag coefficients for a cascade of airfoils and are substituted in Eq. 3.4 to calculate the resultant force coefficient along the track. The force along the track per airfoil can then be obtained using Eq. 3.5.

$$F_T = \frac{1}{2} \rho U_\infty^2 c S C_F \tag{3.5}$$

For n airfoils along the front side of the triangular track, an approximation for the total force along the track is nF_T. The exact value can be determined by using the numerical data from Fluent. It is expected that the top and bottom airfoil along the track will have a large contribution to the total force than the middle airfoils**.** The total power generated along the ascending track with n airfoils is given by Eq. 3.6, excluding inefficiencies due to chains and end effects of the wing.

$$P = nF_T U_T \tag{3.6}$$

3.2 Flow Field Simulation of a Single Airfoil on Ascending Track

3.2.1 Description of NACA 64421 Airfoil

In last several decades, important contributions have been made to provide wind turbine manufacturers with superior airfoil families such as NACA 64 series of airfoils that fulfill the intrinsic requirements in terms of design point performance, off-design capabilities and structural properties [6].

The NACA 63 and 64 six-digit series airfoils are still being used for wind turbine blades. These airfoils have been optimized for high speed wind condition to achieve higher maximum lift coefficient for a small range of operating conditions [7, 8]. The NACA 64 series airfoils have an upper surface contoured so as to increase the flow velocity to avoid separation for the desired range of incidence angles. The lower surface is contoured so as to maintain the desired thickness [9].

This study employs NACA66421 airfoil. The maximum lift for the NACA64421 airfoil is generated at an angle of attack of approximately 12 degrees. Therefore, this angle of attack is chosen as the design angle of attack for the LAWT. The baseline forward track angle is chosen as 60 degrees and a wind speed of 14 m/s is considered. For steady-state operation with track speed equal to wind speed, the freestream velocity seen by the airfoil from Eq. (1) is also 14 m/s. The chord length used in the LAWT design is 0.3 m. From the lift curve and drag polar data available in Ref. [10], the C_L and C_D for the NACA 64421 airfoil at an angle of attack of 12 degrees are approximately 1.2 and 0.12 respectively. It should be noted that the Reynolds number (Re) of the LAWT in this study is approximately one-tenth of the Re used in the experiment in Ref. [10] to obtain these values of C_L and C_D. However, Ref. [10] shows only a slight dependence of the lift curve slope on the Re at an angle of attack of 12 degrees. Therefore, in the absence of data at the actual LAWT Re, the values of 1.2 and 0.12 for C_L and C_D respectively are used to validate the numerical approach.

3.2.2 Computational Fluid Dynamics (CFD) Methodology

All the simulations in this thesis employ the Computational Fluid Dynamics (CFD) methodology to compute the flow field. CFD is a branch of fluid mechanics which numerically solves the governing equations of fluid dynamics.

CFD technology solves the governing equations of fluid dynamics which include the continuity equation, the Naiver-Stokes equations and the energy equation. Given the complexity and nonlinearity of the Naiver-Stokes equations, depending upon the appreciation and physics of the problem, they are often simplified by invoking several assumptions. The equations are simplified by assuming the fluid to be inviscid and therefore deleting the viscous terms to yield the Euler equations. By making addition assumption that the fluid flow is irrotational, one obtains the full potential equation. Finally, for small perturbations in subsonic and supersonic flows (not transonic or hypersonic) the full potential equation can be linearized to yield the linearized potential equation [9].

The basic procedure employed in obtaining the CFD solution is Pre-processing, Flow field simulation and Post-processing. Pre-processing includes geometry modeling, mesh generation about the body, and boundary conditions at various boundaries of the flow domain. The governing

equations are discretized at mesh points and are solved using an appropriate algorithm on a computer to obtain the values of the flow variables at the mesh points. Post-processing is used for analysis of the computed data and shape optimization.

Most well-known CFD codes that have been developed during past three decades are Fluent, StarC++, Overflow, etc. In this study, the most commonly used CFD solver ANSYS Fluent is employed for flow field simulations.

3.2.3 Turbulence Modeling

Most of the flows encountered in nature and in industrial systems are generally turbulent. Turbulence characterizes the random and chaotic motion of viscous fluid flow at high Reynold numbers. Turbulent flows are characterized by fluctuating velocity, pressure and temperature fields.

Because of small scale and high frequency of the flow fluctuations, it is too difficult and expensive to directly simulate the turbulent flow by solving the Naiver-Stokes equations at high Reynolds numbers for practical engineering applications. Therefore, the instantaneous (time dependent) governing equations are generally time-averaged or ensemble-averaged to remove the small scales, thereby resulting in a time-averaged set of equations that are computationally less intensive to solve. These equations are known as the Reynolds-Averaged Naiver-Stokes (RANS) equations. Unfortunately, the RANS equations contain additional unknown variables known as the "Reynolds-Stresses" that need to be modeled. Therefore, turbulence models are needed to define these stresses in terms of known quantities (flow variables) [9].

There are several most commonly used turbulence models, e.g., the Spalart-Allmaras (SA) Model, the Shear-Stress Transport (SST) k-ω model and k-kl-ω Transition model.

In this study, accurate simulation of LAWT airfoil is relatively difficult because of lower Reynolds number at which the laminar flow at the leading edge of the airfoil tends to separate and becomes transitional before becoming fully turbulent [10]. The process of a laminar flow becoming turbulent is known as laminar-turbulent transition. This is an extremely complex process which even today is

not fully understood. However, as a result of several decades of excellent research, certain features of transitional flow have become gradually clear, and it is now known that the process develops through a series of instability modes. While transition can occur in any fluid flow, it is most often important in the context of boundary layers.

To solve the transitional flow over the airfoil at relatively lower Reynolds number (in transitional region), in this study, k-kl-ω turbulence model was used to account for the laminar-turbulent transition region on the airfoil [11]. This model has been found to be fairly accurate for predicting the transition in boundary layer flows. It is a three-equation eddy-viscosity type turbulence model.

3.2.4 Mesh Generation

Mesh is a mathematical representation of a set of discrete points in the computational domain which is needed to discretize the governing equations of fluid flow at these points. The commercially available software ANSYS ICEM is employed to generate a structured mesh around a single airfoil.

There are two types of mesh which are most commonly used: O-grid and C-grid as shown on Fig. 3.3 and Fig. 3.4. For viscous flow, a C-grid is preferred because it allows to resolve the wake more accurately. C-grid is aligned to the wake or slipstream at the trailing edge of the airfoil. In particular, for grid adaptation, for viscous flow past an airfoil, it is easier to resolve a boundary layer and the wake with a C-grid.

The mesh used in this study has a C-grid topology. The grid is refined near the leading edge and trailing edge and is adapted to the flow gradients. The mesh is generated using ANSYS ICEM.

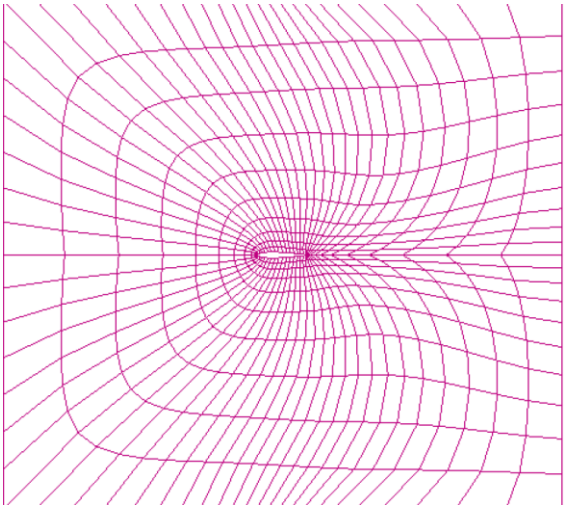

Figure 3.3: C-grid Mesh around the Single Airfoil (Zoomed-in View)

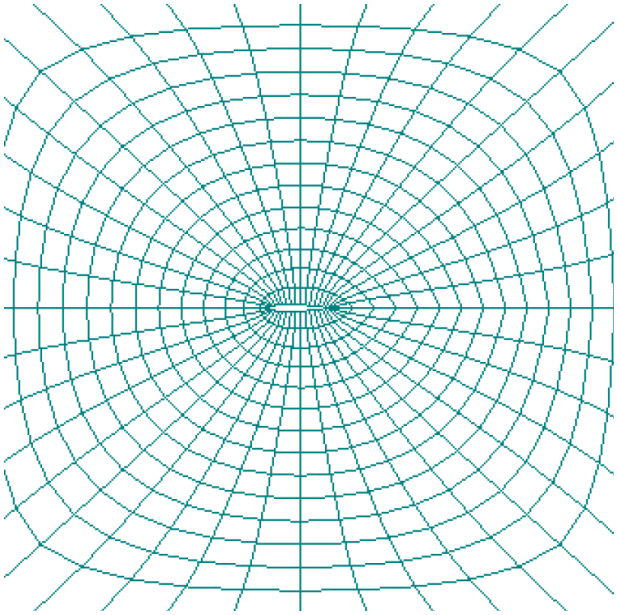

Figure 3.4: O-grid Mesh around the Single Airfoil (Zoomed-in View)

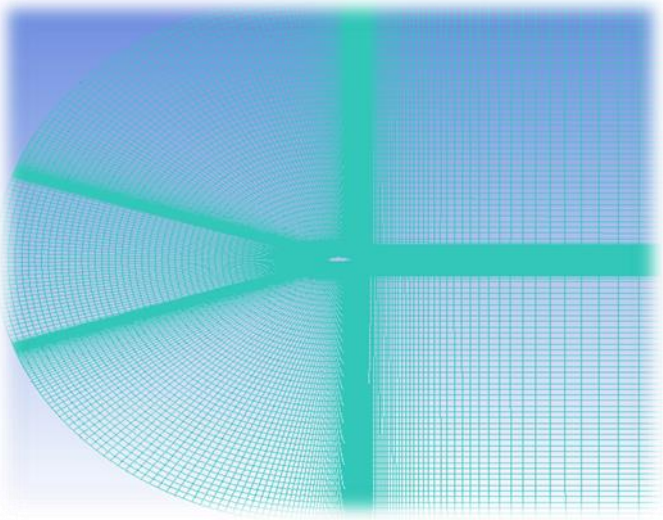

Figure 3.5: Adapted Mesh around the Single Airfoil in Computational Domain

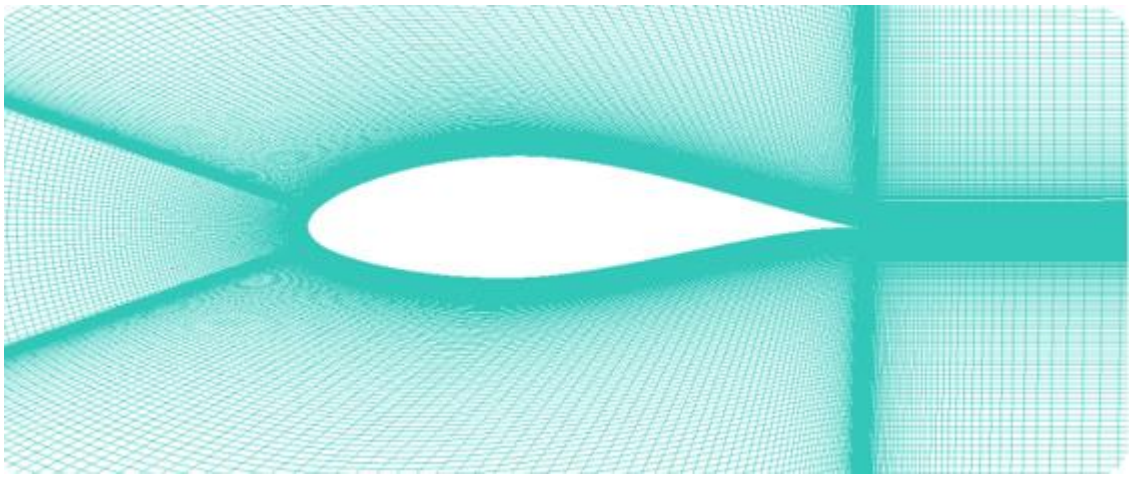

Figure 3.6: Zoomed-in View of Adapted C-Grid Around the NACA 64421 Airfoil

Fig. 3.5 shows the mesh around the NACA 64421 airfoil. In this mesh, there are 76,725 quadrilateral cells and 77,256 nodes. The far field boundary is set at 15 chord lengths.

The airfoil mesh is imported into ANSYS Fluent to solve for the flow field and to obtain the lift and drag coefficients. As mentioned before, to account for flow in the laminar-turbulent transition region, the k-kl-ω turbulence model is used throughout this study [12]. The flow is assumed to be steady and incompressible. Adaptive meshing is employed to maintain y+ values under 1 next to the airfoil surface to ensure the accuracy of the numerical solution.

3.2.5 Flow Field Results

The plot of the pressure coefficient for the NACA 64421 airfoil is shown in Fig. 3.7. Pressure contour and velocity contours are given in Fig. 3.8 and Fig. 3.9 respectively. The computed values of C_L and C_D from ANSYS Fluent are 1.196 and 0.104 respectively. These values match the empirical data from Ref. [4] and thus validate the present numerical solution.

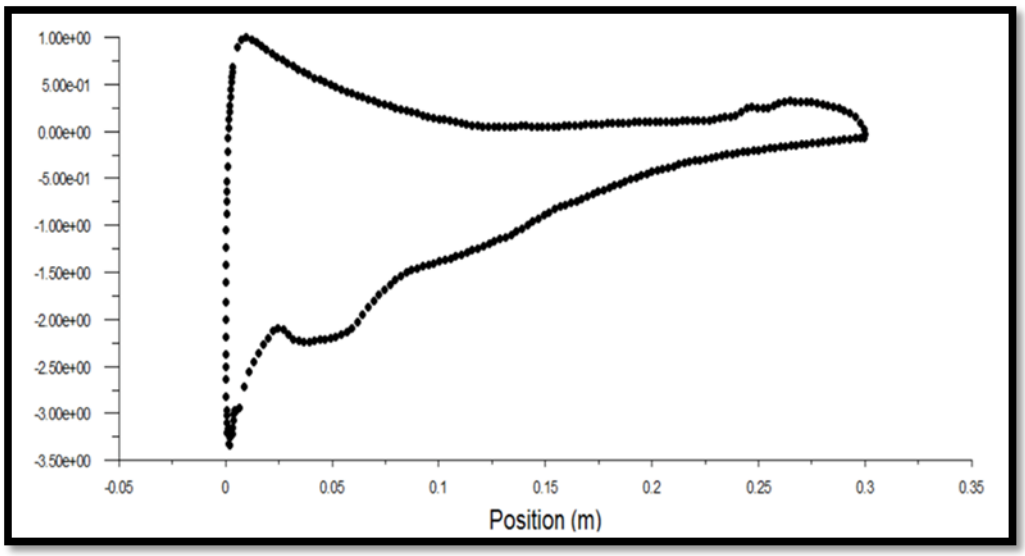

Figure 3.7: Pressure Coefficient Distribution for Single Airfoil on Ascending Track, $Re_{C=0.3m}$ = 315,221, α = 12 degrees

3.3 Flow Field Simulation of Cascade of Airfoils on Ascending Track

3.3.1 Modeling Setup

For a given LAWT configuration, there is a certain number of wings on the ascending track spaced some distance apart. This section investigates the effect of stacking airfoils along the track for the LAWT configuration. In this section, simulations of a cascade of 3 to 19 NACA 64421 airfoils are conducted using ANSYS Fluent. The goal of this study is to establish trends in average lift and drag coefficients versus the number of airfoils so that the average lift and drag can be accurately estimated for any given number of airfoils. The cases considered consist of a cascade of 3, 4, 5, 10,

and 19 airfoils respectively. The spacing between the airfoils along the track direction is set equal to the chord length of 0.3 m**.**

The mesh for the cascade of airfoils is generated in ANSYS ICEM using a block-grid approach repeated for each airfoil of the cascade. The mesh has a C-grid topology around each airfoil of the cascade. Fig. 3.8 and Fig. 3.9 show the mesh around three airfoils. In this mesh, there are 410,777 quadrilateral cells and 419,372 nodes. The far field boundary is set at 15 chord lengths. Once the mesh is imported into ANSYS-Fluent, adaptive meshing is employed to ensure that the y+ value is less than 1 next to the surface of the airfoils.

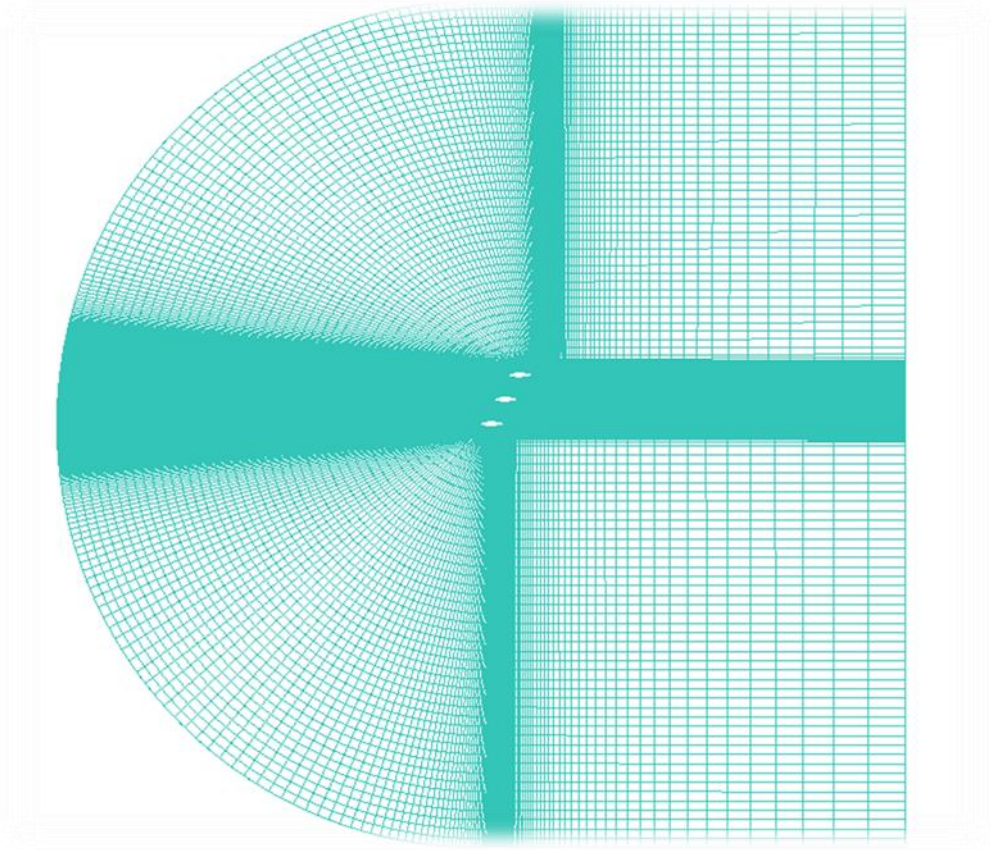

Figure 3.8: C-grid Around a Cascade of Three Airfoils

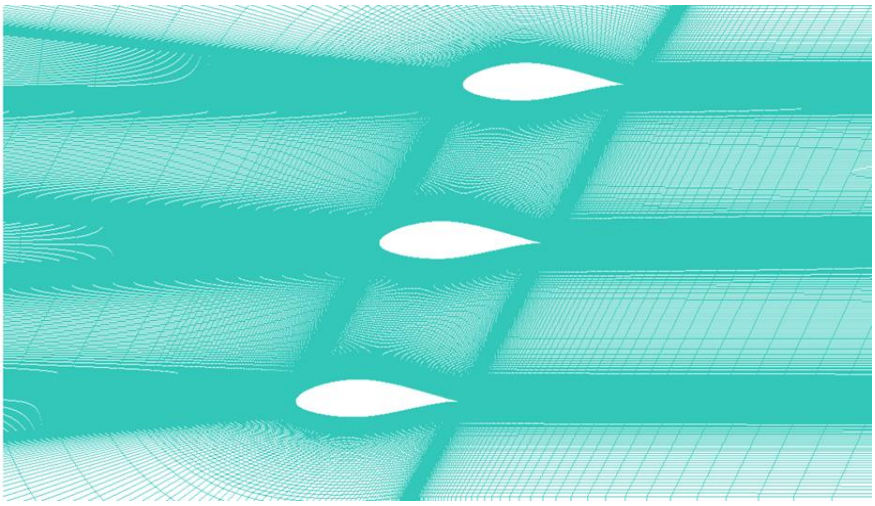

Figure 3.9: Zoomed-in View of C-grid Around a Cascade of Three Airfoils

3.3.2 Calculation of Total Lift and Drag of LAWT on Ascending Track

For a given LAWT, there are n airfoils on the ascending track. It is important to determine the average lift and drag coefficient to get the overall lift and drag force which will finally contribute to the power generation from a LAWT.

It is assumed that the middle airfoil of the cascade represents the rest of the airfoils since it can experience the average aerodynamic effect of having equal number of airfoils on both sides. Once the aerodynamics of the middle airfoil is determined it would then be possible to use this result for any other airfoil around the loop. Thus an equation for the total coefficient of lift can be written as: C_L (total) = C_L (top) +C_L (bottom) + (n-2) C_L (middle).

To calculate the average of total lift and total drag, five cases are considered. These cases are simulated in ANSYS- Fluent with a cascade of: 3 airfoils, 4 airfoils, 5 airfoils, 10 airfoils and 19 airfoils. These five cases provide a variation of average C_L and C_D with number of airfoils. Viewing the trend of average C_L and C_D from the five cases, the total lift and drag coefficient of a LAWT can be calculated.

The meshes around 4, 5, 10 and 19 airfoils in the cascade are generated in a similar manner in ANSYS-ICEM. Each simulation is run with a freestream velocity of 14 m/s with an angle of attack of 12 degrees. The k-kl-ω turbulence model is used in the simulations and the flow is assumed to be steady and incompressible in each case.

3.3.3 Results and Discussion

The pressure coefficient distributions over each airfoil for a cascade of 3, 4 and 5 airfoils are shown in Fig. 3.10, Fig. 3.11 and Fig. 3.12 respectively. The pressure contours and velocity contours for a cascade of 3 and 4 airfoils are shown on Fig.3. 13 to Fig. 3.16 respectively.

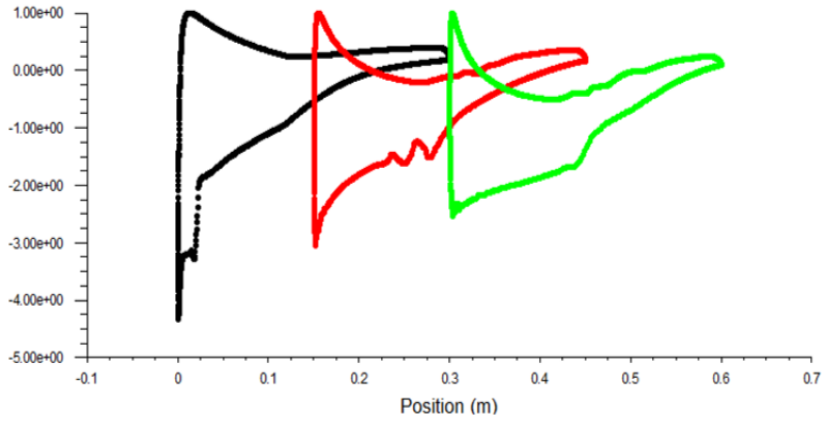

Figure 3.10: Pressure Coefficient Distribution for Cascade of 3 Airfoils, $Re_{C=0.3m}$ = 315,221, α = 12 degrees

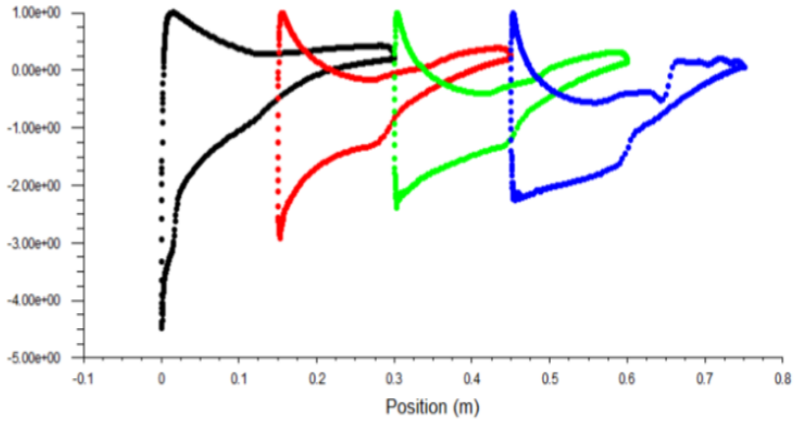

Figure 3.11: Pressure Coefficient Distribution for Cascade of 4 Airfoils, $Re_{C=0.3m}$ = 315,221, α = 12 degrees

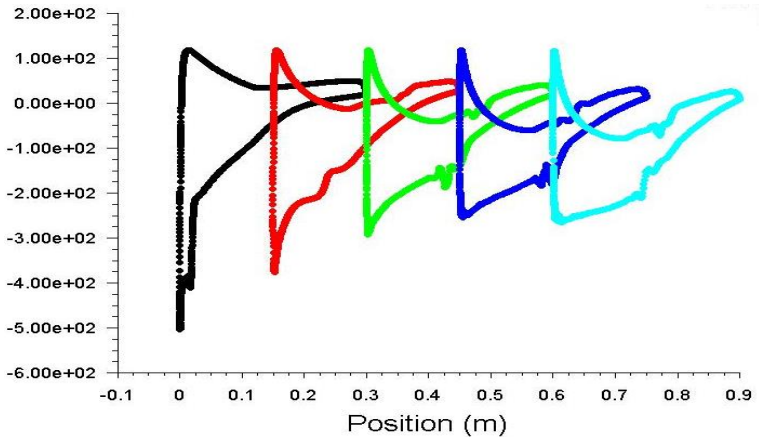

Figure 3.12: Pressure Coefficient Distribution for Cascade of 5 Airfoils, $Re_{C=0.3m}$ = 315,221, α = 12 degrees

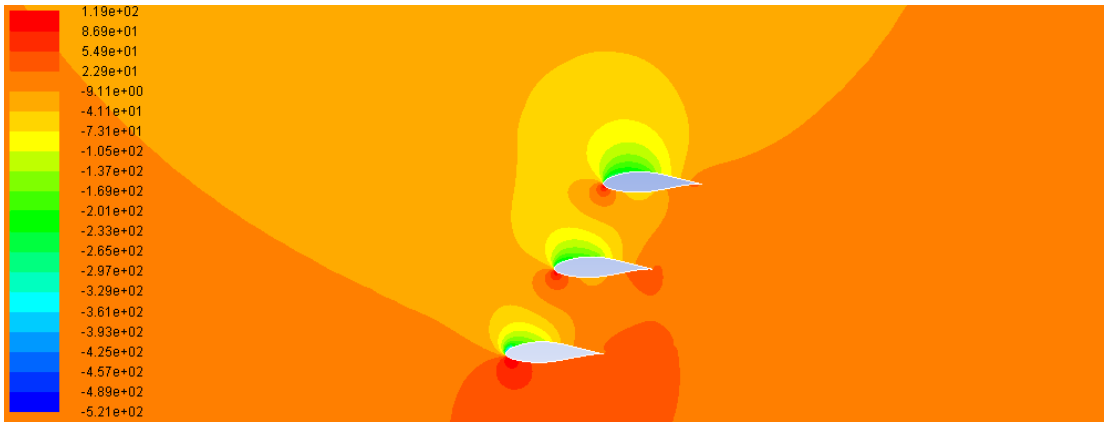

Figure 3.13: Pressure Contours for a cascade of 3 Airfoils at an Angle of Attack =12 degrees

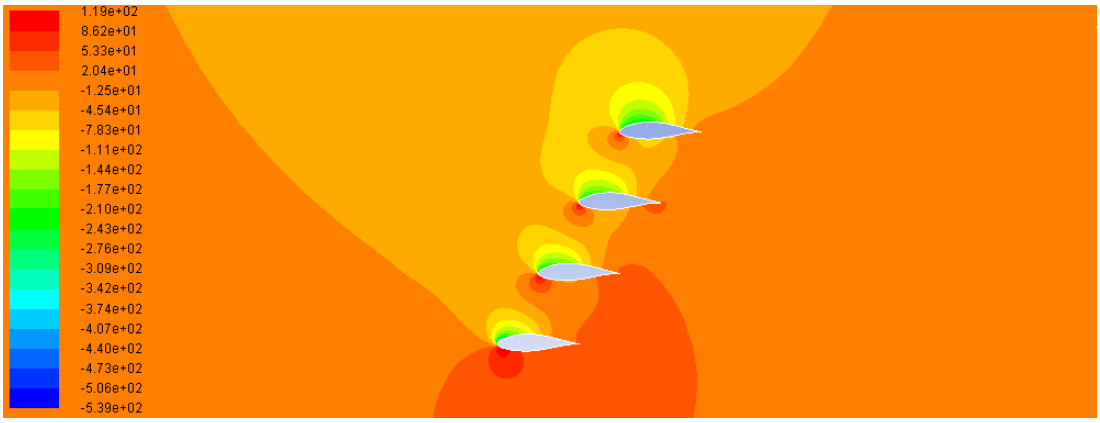

Figure 3.14: Pressure Contours for a cascade of 4 Airfoils at an Angle of Attack =12 degrees

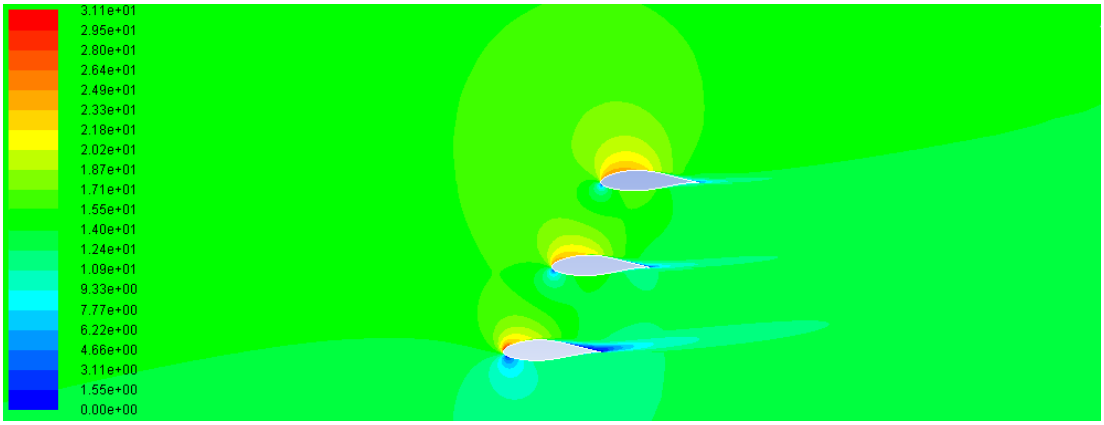

Figure 3.15: Velocity Contours for a cascade of 3 Airfoils at an Angle of Attack =12 degrees

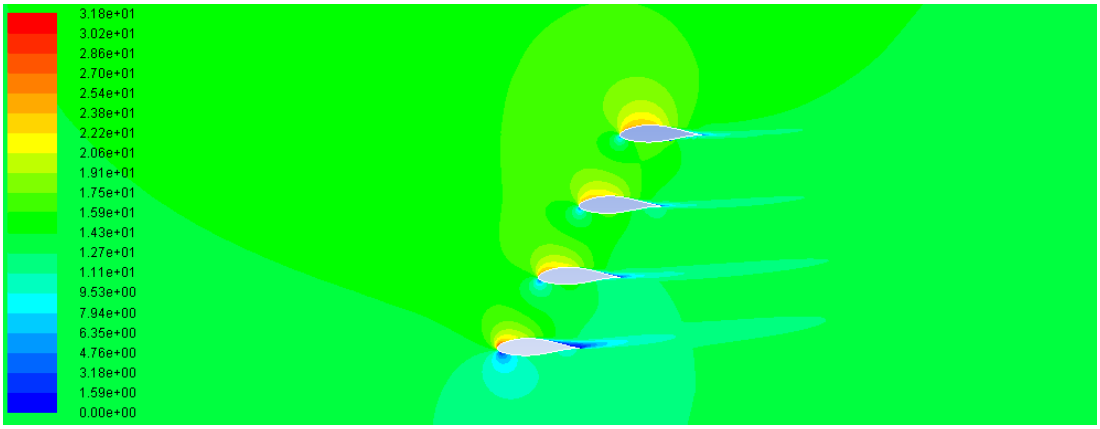

Figure 3.16: Velocity Contours for a cascade of 4 Airfoils at an Angle of Attack =12 degrees

The lift and drag coefficients for each airfoil in the cascade of 3, 4, 5, and 10 airfoils are given in Tables 3.2 and 3.3 respectively, Table 3.4 shows the average lift and drag coefficients for all 5 cases. The first row in the tables refers to the bottommost airfoil.

Table 3.2: Lift Coefficient for Each Airfoil in the Cascade

Number of airfoils in cascade			
3	4	5	10
1.246	1.255	1.190	1.013
1.138	1.078	1.121	1.013
1.138	0.992	0.989	0.984
-	1.046	0.956	0.967
-	-	1.037	0.931
-	-	-	0.883
-	-	-	0.818
-	-	-	0.795
-	-	-	0.786
-	-	-	0.976

Table 3.3: Drag Coefficient for Each Airfoil in the Cascade

Number of airfoils in cascade			
3	4	5	10
-0.040	-0.054	-0.068	-0.075
0.041	0.027	0.011	-0.027
0.084	0.059	0.045	0.005
-	0.088	0.066	0.028
-	-	0.094	0.044
-	-	-	0.056
-	-	-	0.061
-	-	-	0.074
-	-	-	0.079
-	-	-	0.101

Table 3.4: Average Lift and Drag Coefficient with Different Numbers of Airfoils in Cascade

Number of Airfoils	Average C_L	Average C_D
3	1.174	0.0284
4	1.093	0.0299
5	1.063	0.0312
10	0.914	0.0344
19	0.766	0.0540

The assumption that the middle airfoil gives a good representation of the rest of the airfoils in the cascade. As given in Tables 3.2 and 3.3 and comparing it with the average values in Table 3.4, for each cascade, the lift coefficient is the highest for the bottom most airfoil and then decreases along the cascade, except for the top most airfoil which shows a slight increase again. On the other hand, the drag coefficient starts out with a negative value and increases along the cascade such that the topmost airfoil has the highest drag coefficient. The negative drag coefficient on the bottom most airfoils in the cascade is caused by the large static pressure on the bottom surface that cannot be balanced by the pressure on the top surface due to the presence of additional airfoils. This unbalanced pressure overwhelms the viscous drag to produce a net force back towards the freestream velocity on the bottom most airfoils.

Based on the average lift and drag coefficients in Table 3.4, the trends in the average lift and drag coefficient versus the number of airfoils can be identified. These are plotted in Figs. 3.17 and 3.18 respectively. From Fig. 3.17, it can be seen that the average lift coefficient has a negative power law

dependence with respect to the number of airfoils. On the other hand, Fig. 3.18 shows that the average drag coefficient increases linearly with the number of airfoils. It should be noted that although the average lift per airfoil decreases as the number of airfoils is increased, the total lift (and hence, power) still increases. The results in this section can be used to predict the average lift and drag coefficients for any number of airfoils and to calculate the total power from LAWT using Eqs. 3.4-3.6. Using the general formula for average lift and drag for the case of 30 airfoils along the track and assuming a span of 1 m and properties of air at sea level, the power generated by the LAWT is approximately 8.45 kW, which agrees with values reported in Ref. [3].

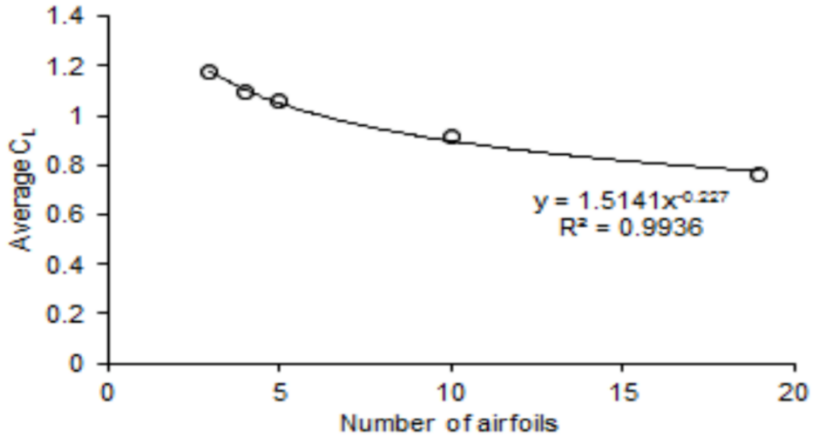

Figure 3.17: Average Lift Coefficient Versus the Number of Airfoils in the Cascade for NACA 64421 Airfoils

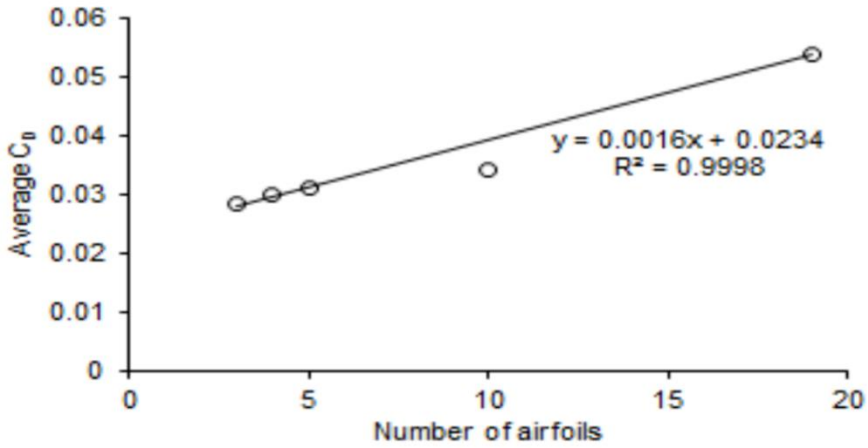

Figure 3.18: Average Drag Coefficient Versus the Number of Airfoils in the Cascade for NACA 64421 Airfoils

3.4 Flow Field Simulation of a Single NACA 64421 Airfoil on Descending Track

3.4.1 Kinematics of Airfoil on Descending Track

The airfoils can extract wind's energy on both ascending and descending track. Based on the design and kinematics of the LAWT, the airfoils on the descending track may contribute an additional force along the track. If the airfoils are fixed with respect to the track, the descending track only contributes to the power when the track speed is below a certain threshold. If the track speed exceeds this threshold, the net angle of attack becomes negative and the net resulting force subtracts from the power generated by the ascending track. However, mechanical pitch adjustments can be added to the LAWT design to ensure that the contribution from the descending track remains positive [3].

The present study considers an airfoil with a fixed pitch that has been flipped to a trailing-edge-first configuration on the descending track as shown in Fig. 3.19. The angle of attack for the flipped airfoil is 20.2 degrees, which corresponds to an airfoil pitch angle such that the ascending angle of attack is the design value of 12 degrees when the track speed is a quarter of the wind speed and both forward and reverse track angles are 60 degrees, as shown in Fig. 3.19. It should be noted that in actual practice, the descending track will lie in the wake of the ascending track and will likely see a reduced wind speed. No attempt has been made to include the effects of the wake in reducing the wind velocity.

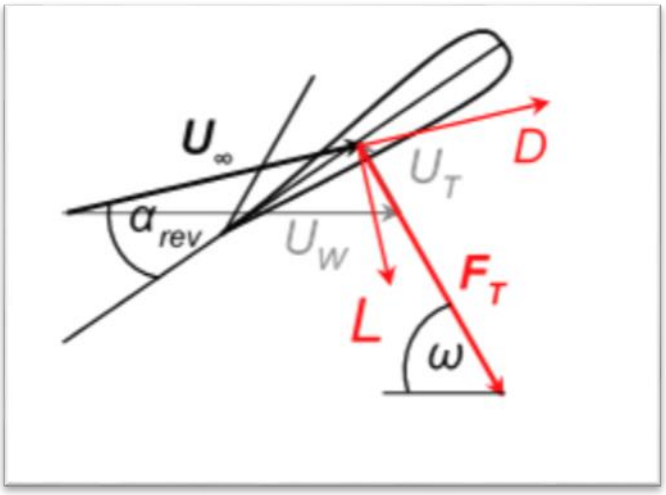

Figure 3.19: Kinematics of LAWT Airfoil on Descending Track with Track Speed Equal to Quarter of the Wind Speed

3.4.2 Results and Discussion

The modeling setup and mesh generation are similar to the cascade of single airfoil on the ascending track. The pressure coefficient distribution obtained by ANSYS-Fluent is plotted in Fig. 3.20. From Fluent, the computed lift coefficient is 0.535 and the drag coefficient is 0.1661. The coefficient of power along the track can be determined using Eq. 3.4 with the forward track angle β replaced by the reverse track angle ω.

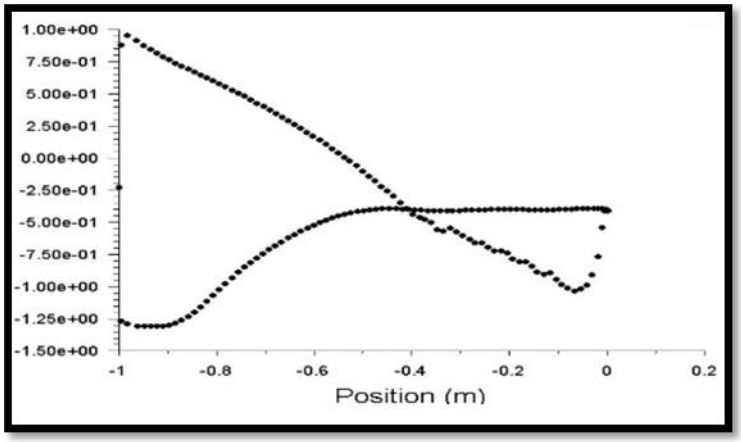

Figure 3.20: Pressure Coefficient Distribution for Single Airfoil on Descending Track, $Re_{C=0.3m}$ = 315,221, α = 20.2 degrees

The lift coefficient for the flipped airfoil on the descending track is considerably less than that of the single airfoil on the ascending track; on the other hand, the drag coefficient is much higher. This is expected because the flow encounters the sharp trailing edge of the airfoil first and then separates leading to a stall condition, which reduces lift and increases drag. This is verified from the velocity contour shown in Fig. 3.21. The velocity contour shows a prominent zone of separation of the sharp edge. These results indicate that the drag can also be a significant contributor to the resultant force along the descending track.

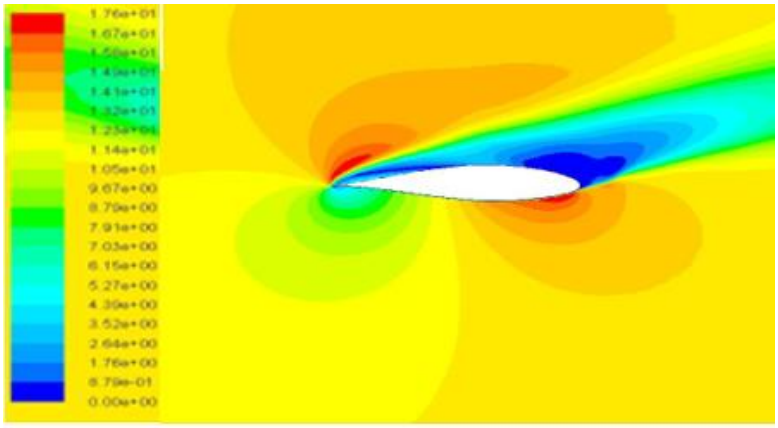

Figure 3.21: Velocity Contour for the Flipped Airfoil on the Descending Track at an Angle of Attack = 20.2 degrees

3.5 Optimization Methodology for LAWT Design

For a given C_L and C_D, the effects of the various angles, namely the angle of attack and pitch angle, in the LAWT design have already been accounted for in the analytical formulation of power via Eqs. 3.4-3.6. However, it is expected that the C_L and C_D are also affected by the track angle β and the spacing between the airfoils.

The objective of this section is to identify the design parameters that have the biggest effect on power generation from LAWT and then optimize them. Fig. 3.22 schematically illustrates the optimization methodology.

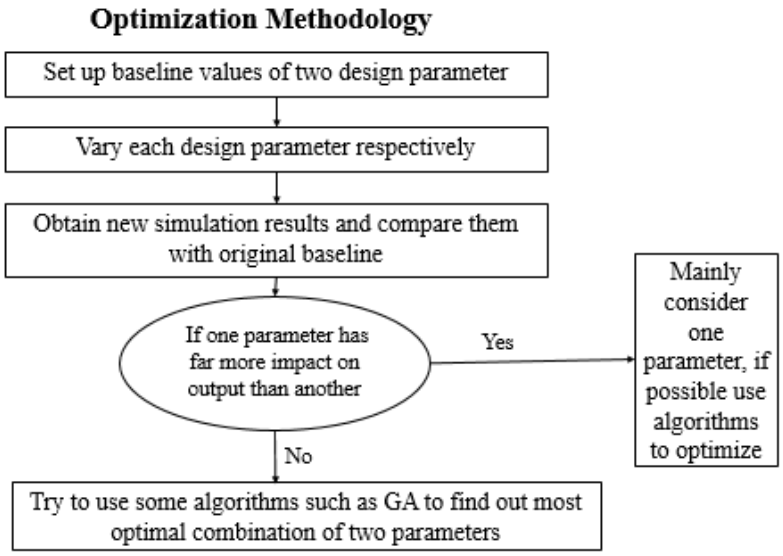

Figure 3.22: Schematic of Information Flow in Optimization Process

For this purpose, various numerical studies are conducted by varying the forward track angle and the spacing between airfoils The track angle of 60 degrees and spacing of one chord length between the airfoils is considered as the baseline case (case 0). Four cases are investigated which are summarized in Table 3.5. It should be noted that in each of these cases, a cascade of 3 airfoils is considered. Each simulation is run with a freestream velocity of 14 m/s with an angle of attack of 12 degrees. The k-kl-ω turbulence model is used in the simulations and the flow is assumed to be steady and incompressible.

Table 3.5: Summary of Cases Run for Various Track Angles and Spacings between the Airfoils

Case	0	1	2	3	4
Spacing	1c	1c	1c	1.25c	0.75c
β (deg)	60	75	45	60	60

3.6 Results and Discussion

For each case in Table 3.5, the lift and drag coefficients for each airfoil in a cascade of 3 airfoils is obtained from the numerical simulation. The average lift and drag coefficients, and the coefficient of the resultant force along the track direction are computed and are given in Table 3.6.

Table 3.6: Results of Numerical Simulations for Case 0, 1, 2, 3and 4 in Table 3.5

Case	0	1	2	3	4
Spacing	1c	1c	1c	1.25c	0.75c
β (deg)	60	75	45	60	60
φ (deg)	60	52.5	67.5	60	60
Average C_L	1.174	1.240	1.083	1.237	1.043
Average C_D	0.028	0.027	0.040	0.030	0.030
Average C_F	1.003	0.968	0.986	1.056	0.889
Average C_F per unit chord of spacing	1.003	0.968	0.986	0.845	1.182

The pressure contours and velocity contours for varies cases are shown in Fig. 3.23 to Fig .3.30.

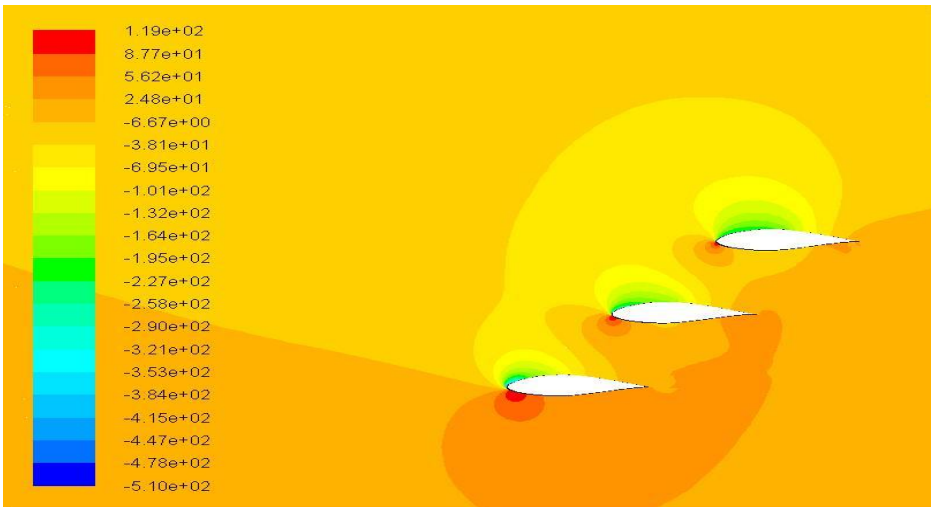

Figure 3.23: Pressure Contours for Case 2 with Spacing 1c and Track Angle 45^0

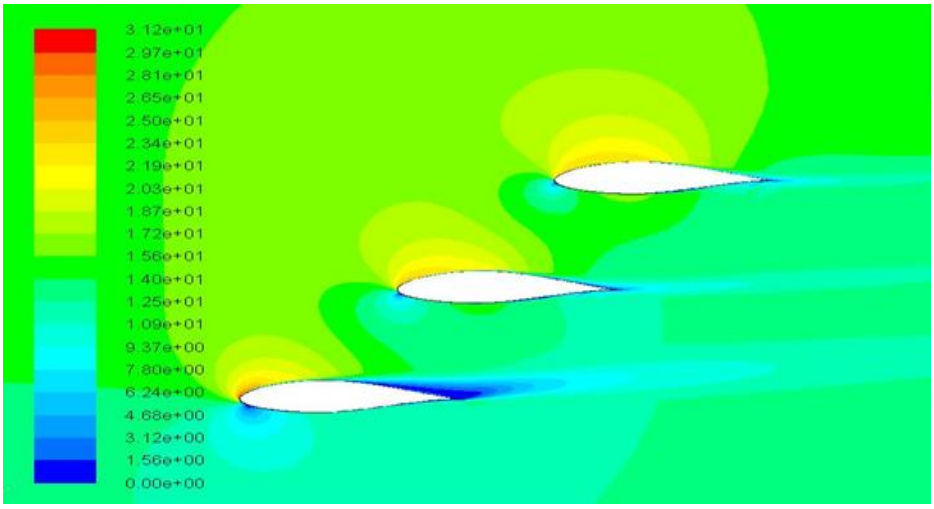

Figure 3.24: Velocity Contours for Case 2 with Spacing 1c and Track Angle 45^0

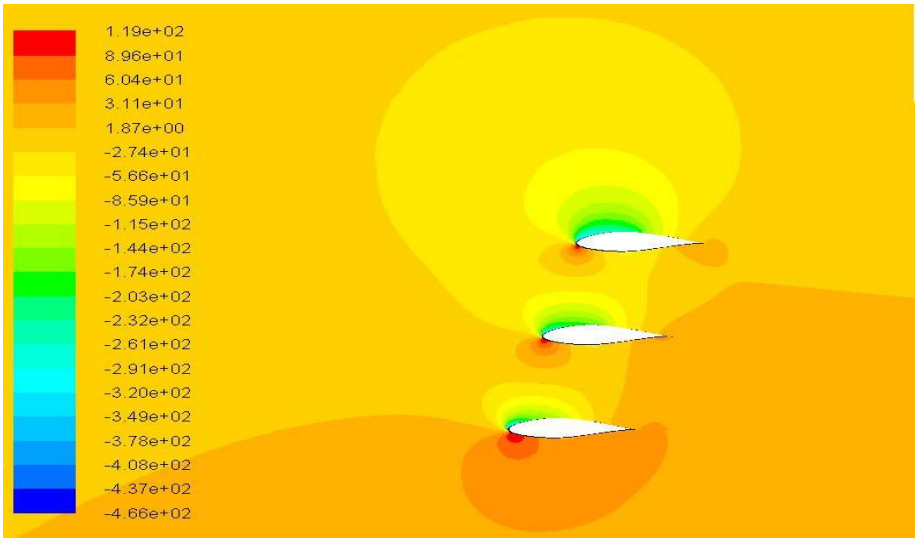

Figure 3.25: Pressure Contours for Case 1 with Spacing 1c and Track Angle 75^0

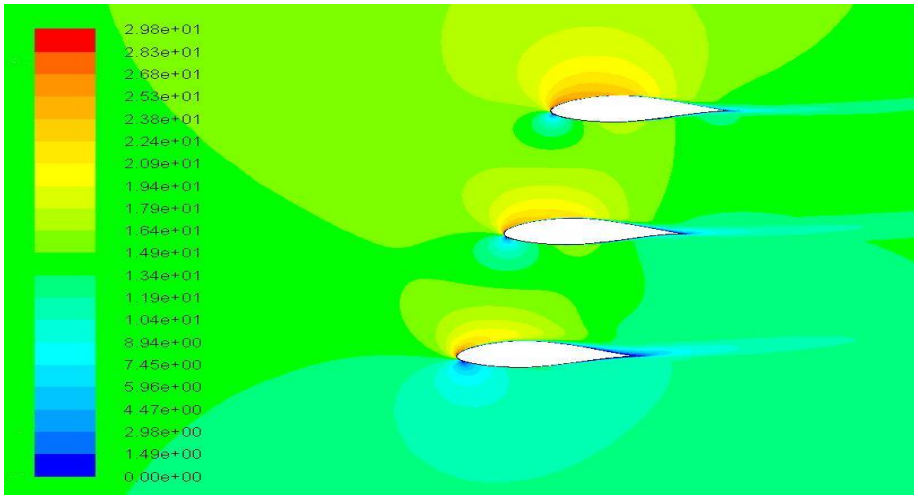

Figure 3.26: Velocity Contours for Case 1 with Spacing 1c and Track Angle 75^0

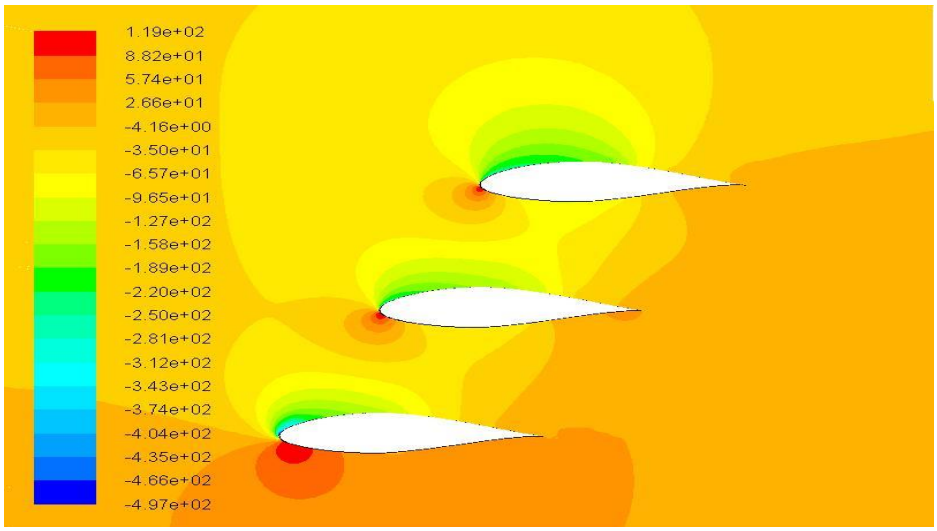

Figure 3.27: Pressure Contours for Case 4 with Spacing 0.75c and Track Angle 60^0

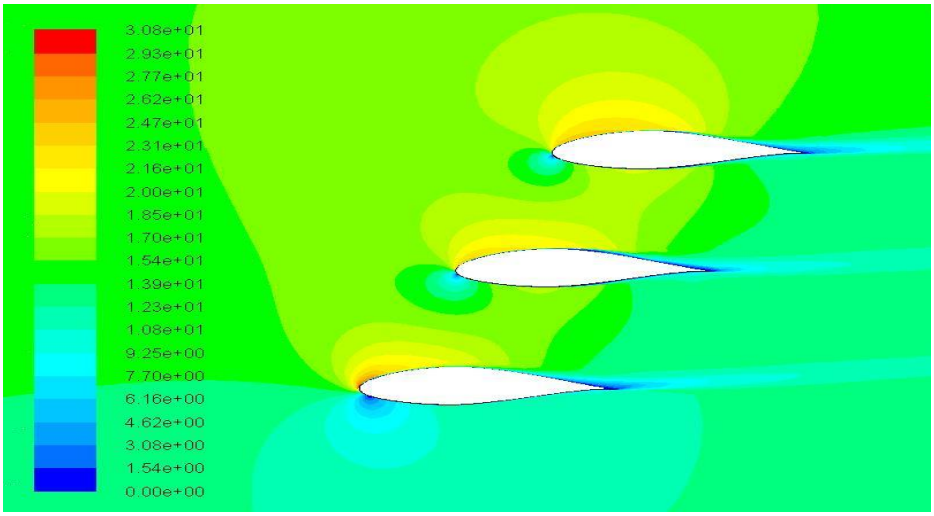

Figure 3.28: Velocity Contours for Case 4 with Spacing 0.75c and Track Angle 60^0

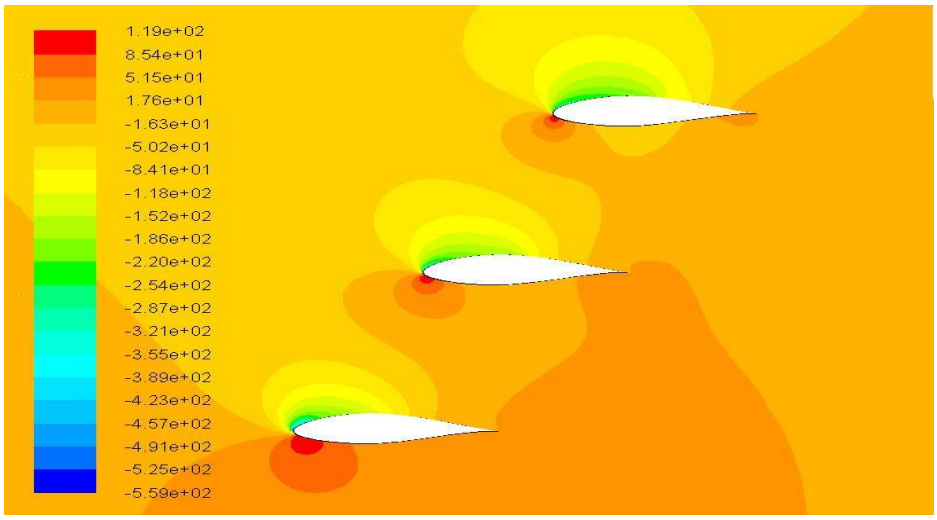

Figure 3.29: Pressure Contours for Case 3 with Spacing 1.25c and Track Angle 60^0

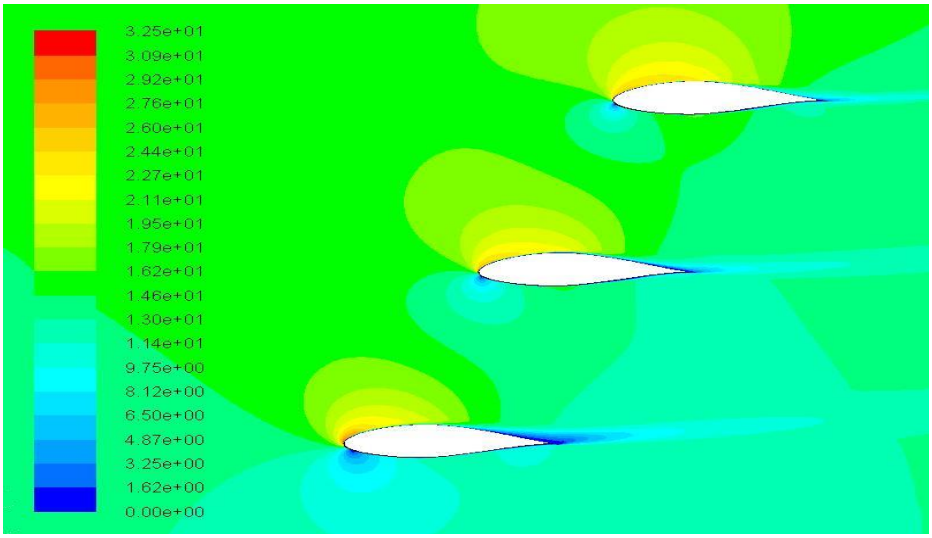

Figure 3.30: Velocity Contours for Case 3 with Spacing 1.25c and Track Angle 60^0

For cases 0, 1, and 2, the spacing and hence the number of airfoils remains constant. From Eqs. 3.5 and 3.6, the total power is therefore directly proportional to the average coefficient of force along the track. Thus, it can be seen that the forward track angle of 60 degrees is the optimal case. The average C_F for both cases 1 and 2 is lower than the average C_F for case 0. It should be noted that although the average C_L for case 1 is greater compared to case 0, the lift acts along a direction such that it has a smaller component in the direction of the track. This result was verified in the original patent that the optimal track angle for the ascending track is 60 degrees for maximum power generation from LAWT.

The results for the cases 3 and 4 with varying spacing between airfoils are of greater interest. From Table 3.6, case 3 with a spacing of 1.25c has the highest average C_F whereas case 4 with a spacing of 0.75c has the lowest average C_F. However, the spacing also affects the number of airfoils that can be placed along the same length of the track. Assuming a track length that fits 30 airfoils with a baseline spacing of 1c, increasing the spacing to 1.25c would reduce the number of airfoils to 24 while reducing the spacing to 0.75c would increase the number of airfoils to 40. Taking this into account, the average C_F per unit chord of spacing shows that case 4 would have greater power generation according to Eq. 3.6 by 18% compared to the baseline case. These results show that significant increases in power generation can be obtained by optimizing the design of the LAWT, particularly the spacing between the airfoils.

It appears that as the spacing between the airfoils becomes smaller, the power increases. However, the spacing between the two airfoils cannot be too small due to negative effects of aerodynamic interference. NACA 64421 is very thick airfoil; the effects of aerodynamic interference cannot be ignored if the two thick airfoils are very close. The simulation results show that if the spacing is half of the chord length (0.5c), the lift coefficient drops significantly. Therefore, it is assumed that the optimal spacing is between 0.5c and 0.75c. To verify this conclusion, two additional cases are simulated.

Table 3.7: Summary of Parameters for Two Additional Cases

Case	0	5	6
Spacing	1c	0.6c	0.8c
β (deg)	60	60	60

For case 5 and case 6, the computed average lift, drag coefficients, and the coefficient of the resultant force along the track are given in Table 3.8.

Table 3.8: Results of Numerical Simulations for Case 0, 4, 5 and 6

Case	0	4	5	6
Spacing	1c	0.75c	0.6c	0.8c
β (deg)	60	60	60	60
φ (deg)	60	60	60	60
Average C_F	1.003	0.889	0.834	0.924
Average C_F per unit chord of spacing	1.003	1.182	1.390	1.155

The average C_F per unit chord of spacing shows that case 5 would have greater power generation by 38.6% compared to the baseline case. These results show that the spacing of 0.6c between airfoils is optimal. This results points out that a more advanced optimization method such as a Genetic Algorithm may be helpful in determining the optimum spacing for maximum power generation from a LAWT.

Chapter 4 Flow Field Simulations of NACA 64421 Hydrofoils and New Highly-Cambered Hydrofoils for LAHT

4.1 Flow Field Simulations of a Single Hydrofoil on Ascending Track of LAHT

LAWT concept can work well both in air and water. Hence the same idea as described in chapter 3 for a LAHT is applied to study an analogous floating Looped Airfoil Hydro Turbine (LAHT) which converts the kinetic energy of river streams into electricity. Like LAWT, the floating LAHT also brings same advantages of a superior lift force of linearly traveling wing to harvest energy from a flowing water stream**.** Since water is approximately 800 times denser than air, it is appears that a LAHT could harvest more energy than a LAWT (See Eq. 3.6). The model of a floating LAHT is shown in Fig. 4.1.

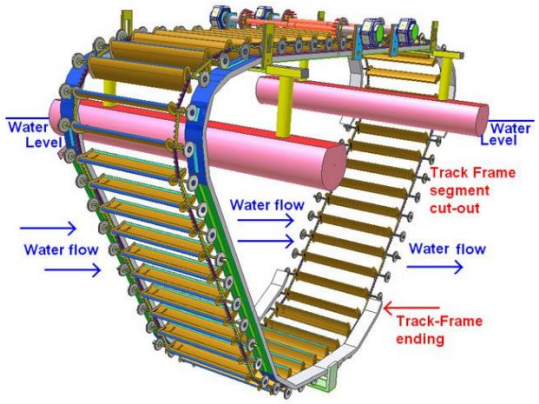

Figure 4.1: Model of a Floating LAHT

The speed of water in a river stream can vary from close to 0 meter per second to 3 meter per second. Factors that affect the speed of water in a river include the slope gradient, the roughness of the channel and effects of tides. In this study, the water speeds of 1 m/s and 3 m/s are chosen for the simulation.

First a uniform wing of NACA66421 airfoil section is considered. The results in chapter 3 for a LAWT showed that the maximum lift for the NACA64421 airfoil is generated at an angle of attack of approximately 12 degrees. Therefore, for a LAHT, an angle of attack of 12 is chosen along with the forward track angle of 60 degrees as the baseline case.

For water speed of 1.3 m/s, the computed value of C_L and C_D from ANSYS-Fluent are 1.57 and 0.03 respectively. Comparing these values with those for a LAWT, it can be noted that the results for a LAHT are better as shown in Table 4.1. In Table 4.1, the results for LAWT are for wind speed of 14m/s while the results for LAHT are for water speed of 1.3m/s. For higher water speed, the results for a LAHT will be much superior.

Table 4.1: Comparison of Performance Between Single Airfoil and Hydrofoil

	C_L	C_D
Single Airfoil in LAWT	1.196	0.104
Single Hydrofoil in LAHT	1.572	0.031

4.2 Flow Field Simulations of Cascade of Hydrofoils on Ascending Track of LAHT

As in the case of LAWT in chapter 3, for a given LAHT, there is a certain number of hydrofoils on the ascending track with a specific spacing between the airfoils. Again for LAHT, cascades of NACA 64421 hydrofoils are simulated using ANSYS Fluent. In this section, a cascades of NACA 64421 hydrofoils are simulated in ANSYS Fluent. The three cases considered consist of 3, 4, and 5 hydrofoils in the cascade. The spacing between the hydrofoils along the track direction is set at chord length of 0.3m.

The mesh for the cascade of hydrofoils is again generated using ANSYS ICEM. The mesh has an C-grid topology with block grid around each hydrofoil. The far field boundary is set at 20 chord length. Once the mesh is imported into ANSYS-Fluent, adaptive meshing is employed to ensure that the y+ value is less than 1 at a grid point next to the surface of the airfoil. Each simulation is run with a freestream velocity of 1m/s and 3m/s respectively at an angle of attack of 12 degrees. Again, the k-kl-ω turbulence model is employed in the simulations and the flow is assumed to be steady and incompressible.

The lift and drag coefficients for each hydrofoil in the cascade of 3, 4, and 5 hydrofoils are given in Table 4.2 and 4.3 respectively. Table 4.4 shows the average lift and drag coefficients for all three cases. The first row in tables refers to the bottom most hydrofoil.

Table 4.2: Lift Coefficient for Each Hydrofoil in the Cascade

Number of hydrofoils in cascade		
3	4	5
1.273	1.216	1.210
1.117	1.075	1.114
1.123	0.980	0.975
-	1.058	0.933
-	-	1.013

Table 4.3: Drag Coefficient for Each Hydrofoil in the Cascade

Number of hydrofoils in cascade		
3	4	5
-0.040	-0.061	-0.066
0.043	0.029	0.011
0.086	0.058	0.046
-	0.089	0.066
-	-	0.092

Table 4.4: Average Lift and Drag Coefficient for the Cascade with Different Number of Airfoils

Number of Airfoils	Average C_L	Average C_D
3	1.171	0.030
4	1.082	0.0289
5	1.049	0.0298

Like LAWT, for each cascade the lift coefficient is the highest for the bottom most hydrofoil and then decreases for other hydrofoils in the cascade, except for the topmost hydrofoil which shows a slight increase again. The drag coefficient starts out at with a negative value and increases along the cascade such that the top most airfoil has the highest drag coefficient. As in the case of LAWT, the negative drag coefficient on the bottommost is caused by the large static pressure on the bottom surface that cannot be balanced by the pressure on the top surface due to the presence of the additional hydrofoils. This unbalanced pressure overwhelms the viscous drag to produce a net force back towards the freestream velocity on the bottom most hydrofoils.

Based on the average lift and drag coefficients in Table 4.4, the trends in the average lift and drag coefficient versus the number of airfoils are similar to those shown in Figs. 3.18 and 3.19. The average lift per airfoil decreases as the number of airfoils increases; however, the total lift (and hence, power) still increases.

The results for water speed of 1m/s are very close to the results for air speed of 14 m/s. Despite of the fact that the results from water are similar to those from air for the speed considered, LAHT has greater potential for increasing power generation due to higher density of water (800 times greater than air). For example, for a cascade of 3 hydrofoils, when the water speed is 1m/s and 3m/s respectively, the power generated from a 3 hydrofoils LAHT is approximately 4320w and 38880w respectively as given in Table 4.5.

Table 4.5: Comparison of Power Generation Between a LAWT and a LAHT

Cascade of 3 Airfoils or Hydrofoils	Power (w)
LAWT with wind speed of 14m/s	4536
LAHT with water speed of 1m/s	4320
LAHT with water speed of 3m/s	38880

When the water speed is 3m/s, the power generated by a LAHT is 756% more than the power generated by a LAWT. From the results shown in Table 4.5, LAHT performs similar to a normal LAWT when the water speed is slow. If the water speed is fast enough, LAHT performs better than LAWT. Thus, the potential of LAHT appears very promising.

4.3 Flow Field Simulation of a New Highly-Cambered Hydrofoil for LAHT

4.3.1 Introduction of a New Highly-Cambered Hydrofoil

As mentioned in section 3.2.1, the NACA 63 and 64 six-digit series airfoils are still used for wind turbine blades today. These airfoils have been optimized for high speed wind condition to obtain higher maximum lift coefficient and very low drag over a small range of operating conditions [7, 8].

However, for LAWT or LAHT concept which utilizes both lift and drag aerodynamic forces produced by wind energy, NACA 64 six-digit series clearly is not the most ideal airfoil or hydrofoil. To get more drag for a LAWT or a LAHT, a new highly-cambered airfoil or hydrofoil has been designed and built by EverLift Inc. using the NASA foil-simulation applet. The airfoil profile is shown in Fig 4.2.

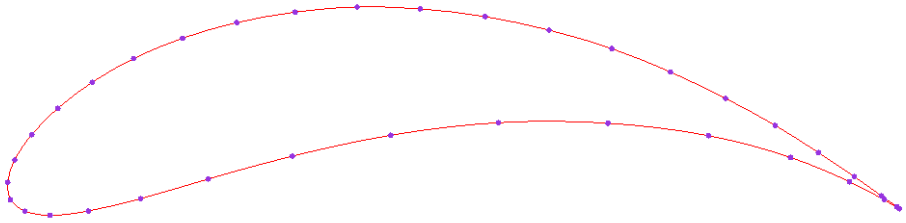

Figure 4.2: Highly-Cambered Airfoil or Hydrofoil

Obviously, this highly-cambered airfoil is not suitable for aviation or aircraft application because of its high drag. However, this highly-cambered airfoil can produce very high lift and drag and therefore is very suitable for LAWT or LAHT application. It should be noted that for LAWT/ LAHT, the high drag coefficient is an extra bonus for LAWT/LAHT in addition to high lift. This airfoil is unsuitable for an airplane wing, thus one cannot find such an airfoil in the NACA library.

4.3.2 Concept of Minimal Spacing between the Hydrofoils

The "minimal spacing between the airfoils or hydrofoils" is the smallest distance between the adjacent airfoils or hydrofoils which results in little aerodynamic interference.

The inventor George Syrovy has researched this issue for many years. Based on the data available for various biplane designs and some tri-plane designs since 1920s, George has concluded that nearly all bi-planes have distance between the wings equal or slightly bigger than the wing chord. It should be noted that even the modern large Russian agricultural spray bi-planes from 1900s used today have the distance between the two wings of about a chord length and also the smaller modern "bush" bi-planes used in Alaska etc.

In order to avoid aerodynamic interference, George Syrovy has suggested the spacing between the blades to be two times of the chord length. He designed the first model of LAWT using a distance of two chord length between the blades; however, it is found by numerical simulations described in chapter 3 that the spacing between the blade should be of the order 0.6 times the chord to extract maximum power from LAWT.

The designed wings of a LAHT model originally built by Syrovy have chord length of 2.45 inches while the distance between them is 5 inches. Thus the distance between the hydrofoils of LAHT model is greater than two chord. In a later model, Syrovy introduced additional 14 thin metal rods between the two blades which could mount additional 14 hydrofoils to reduce the spacing between the blades to be 2.5 inches, approximately equal to the chord.

4.3.3 Flow Field Simulation of a Single Highly-Cambered Hydrofoil

The maximum lift for a highly-cambered hydrofoil is generated at an angle of attack of approximately 17 degrees. Accordingly, this is chosen as the design angle of attack for the LAHT. The baseline forward track angle is chosen as 60 degrees and a water speed of 3 m/s is considered. The chord length used in the simulation of single hydrofoil is 0.3 m. It should be noted that C_L for the highly-cambered hydrofoil at an angle of attack of 17 degrees is approximately 2.8; this value of C_L is validated by the numerical simulation.

The mesh for a single highly-cambered hydrofoil is generated using ANSYS-ICEM. Figs. 4.3 and 4.4 show the mesh. In this mesh, there are 78,375 quadrilateral cells and 78,916 nodes. The far field boundary is set at 20 chord length. Once the mesh is imported into ANSYS-Fluent, adaptive meshing is employed to ensure that the y+ value is less than 1 at all grid points next to the hydrofoil.

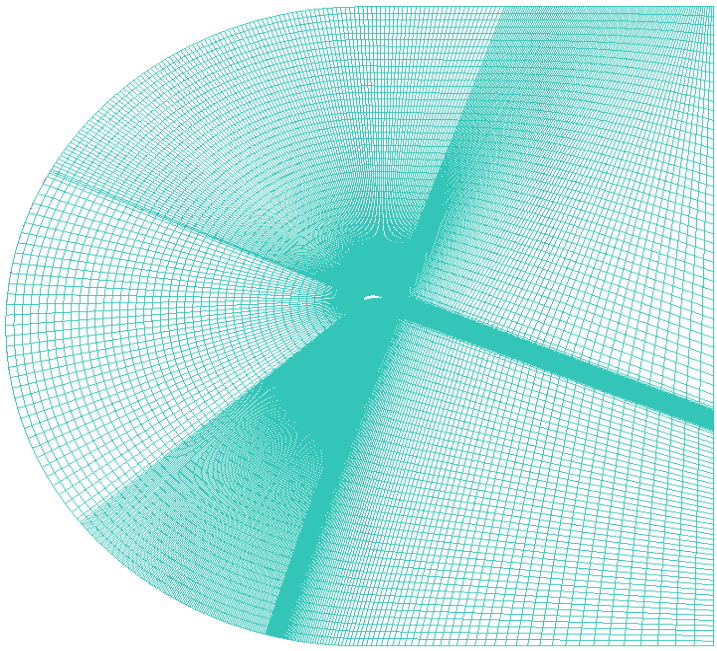

Figure 4.3: Mesh Around the Highly-Cambered Hydrofoil

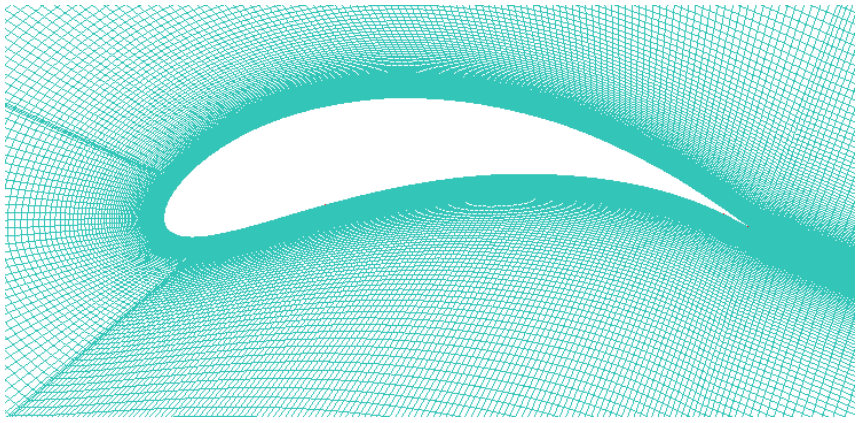

Figure 4.4: Zoomed-in View of the C-grid Around the Highly-Cambered Hydrofoil

ANSYS Fluent is used to solve the flow field and obtain the lift and drag coefficients. The computed value of C_L is 2.98. This value is slightly bigger than the one given by George Syrovy. The computed value of C_D is 0.09. This calculation shows that perhaps a more refined mesh is needed to improve the prediction of lift and drag coefficient.

4.3.4 Flow Field Simulation of a Cascade of Highly-Cambered Hydrofoils

In this section, numerical simulations for a cascade of five hydrofoils are considered with spacing between the blades of one and two chord length.

The mesh around the cascade of hydrofoils is again generated using ANSYS ICEM employing a block-grid approach. Fig. 4.5 and Fig. 4.6 show the structured mesh around five hydrofoils. Again after the mesh is imported into ANSYS-Fluent, an adaptive meshing is employed to ensure that the y+ value is always less than 1 for a grid point next to the hydrofoil surface.

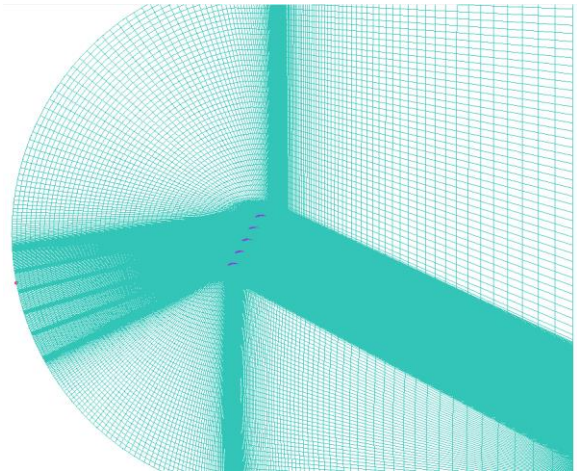

Figure 4.5: Mesh Around a Cascade of Five Highly-Cambered Hydrofoils with Spacing of One Chord Length

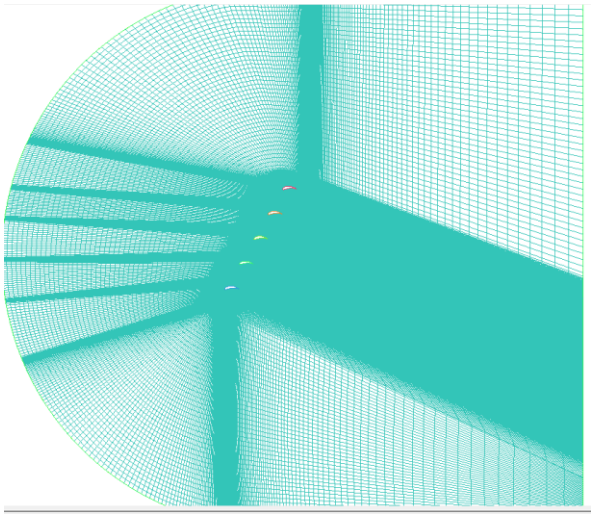

Figure 4.6: Mesh Around a Cascade of Five Highly-Cambered Hydrofoils with Spacing of Two Chord Length

To compare the CFD simulation results with the experimental results from EverLift, the chord length of the hydrofoils in this simulation is taken to be equal to the real model value of 2.45 inch. Thus, two spacings of 2.45 inch and 5 inch are considered in this simulation. Simulation for LAHT are also run for a cascade of 5 NACA 64421 hydrofoils using a chord length of 0.064 meters (2.45 inch).

Three simulation cases are conducted. Case 1 represents the flow simulation of LAHT with a cascade of five NACA 64421 hydrofoils with spacing of one chord length. Case 2 represents flow simulation of LAHT with a cascade of five highly-cambered hydrofoils with spacing of one chord length. Case 3 represents flow simulation of LAHT with five highly-cambered hydrofoils with spacing of two chord length. Table 4.6 shows the results of lift coefficient and drag coefficient for the three cases.

Table 4.6: Results for Three Numerical Simulation Cases

	Case 1		Case 2		Case 3	
	C_L	C_D	C_L	C_D	C_L	C_D
1	1.346	-0.100	1.161	0.202	1.299	0.212
2	1.133	0.004	1.296	0.175	1.873	0.124
3	1.060	0.042	1.736	0.211	2.309	0.168
4	0.998	0.066	1.982	0.181	2.323	0.272
5	1.052	0.092	3.056	0.572	3.034	0.444

Using the C_L and C_D for case 1 and case 2 in Table 4.6, from power generation Eqs. 3.4-3.6, the power generated by the new highly-cambered hydrofoils is 52.95% greater than that generated by NACA 64421 hydrofoils.

Table 4.7: Comparison of Average C_F per unit chord of spacing between Case 2 and Case 3 in Table 4.6

Case	2	3
Spacing	1c	2c
β (deg)	60	60
φ (deg)	60	60
Average C_F	1.846	2.168
Average C_F per unit chord of spacing	1.846	1.084

From Table 4.7, it can be noted that case 3 with a spacing of 2c has higher average value of C_F compared to that for case 2. However, similar to the conclusion in chapter 3, the spacing also affects the number of airfoils that can be placed along the same length of the track. Less spacing means that more hydrofoils can be installed on the track. Thus, case 2 could have additional 5 hydrofoils on the ascending track compared to case 3. The average C_F per unit chord of spacing shows that case 2 thus would have greater total power generation by 72.3% compared to case 3 according to Eq. 3.6.

The above results show that LAHT with spacing of one chord length performs better than that with spacing of two chord length. This spacing can be optimized following the methodology described in section 3.5 to extract maximum power from a LAHT.

In future work, the CFD simulations data should be compared with the experimental data from EverLift Inc. when it becomes available.

Chapter 5 Conclusions

In chapter 3 of this thesis, the mesh generation software ANSYS ICEM and the commercial computational fluid dynamics (CFD) flow solver ANSYS Fluent were employed to simulate the flow field of a single NACA 64421 airfoil. The k-kl-ω turbulence model was used to account for flow in the laminar-turbulent transition region. The computed results matched with the empirical data and thus validated the numerical simulation approach. The numerical procedure was continued to simulate the flow field of a cascade of airfoils on the ascending track of a Looped Airfoil Wind Turbine (LAWT). These results were used to predict the average lift and drag coefficients for any number of airfoils in LAWT and to calculate the total power generated from a given LAWT configuration. The CFD simulations were then conducted to study the flow field of an airfoil on the descending track. It was concluded that the airfoils can extract wind's energy on both the ascending and descending tracks. In the second part of chapter 3, an optimization methodology was employed to determine the optimal track angle and the optimal spacing between the blades to maximize the power generation by the LAWT. In chapter 4, the Floating Looped Airfoil Hydro-Turbine (LAHT) was studied; the results showed that LAHT could generate much greater power compared to LAWT at wind speed of 14 m/s when the water speed is greater than 1 m/s. In this chapter the concept of a highly-cambered airfoil or hydrofoil was also introduced. The computed results showed that this type of airfoil or hydrofoil is best suited for LAWT or LAHT design for best performance.

References

[1] "Efficiency and performance," UK Department for Business, Enterprise & Regulatory Reform, from http://www.berr.gov.uk/files/file17821.pdf, retrieved 2007-12-29.

[2] Banerjee, S., Song, B., and Agarwal, R.K., "Optimization of Looped Airfoil Wind Turbine Design Parameters for Power Generation", Paper No. AJK 2015-28124, ASME-JSME-KSME Joint Fluids Engineering Conference, 26-31 July 2015, Seoul, South Korea.

[3] Syrovy, G.J., "Looped airfoil wind turbine," U.S. Patent 8618682, 2013.

[4] Teschler, L., "Looks like a conveyor, works like a wind turbine," from http://machinedesign.com/batteriespower-supplies/looks-conveyor-works-wind-turbine, retrieved 2013-05-22.

[5] Keller, P.R., "The EverLift LAWT Concept," from https://everliftwind.files.wordpress.com/2014/03/everlift-wintech-article.pdf, retrieved July 2013.

[6] Grasso, F., "Development of Thick Airfoils for Wind Turbines", AIAA Paper 2012-0236, 50th AIAA Aerospace Sciences Meeting, 09-12 January 2012, Nashville, TN.

[7] Timmer, W.A., "An Overview of NACA 6-digit Airfoil Series Characteristics with Reference to Airfoils for Large Wind Turbine Blades", AIAA Paper 2009-268, AIAA 47th Aerospace Sciences Meeting, 05-08 January 2009, Orlando, Florida.

[8] Alexander, G., NACA Airfoil Series., Aerospaceweb.org [cited 2013 March 22nd]; Available from: http://www.aerospaceweb.org/question/airfoils/q0041.shtml.

[9] Chen, X., "Optimization of Wind Turbine Airfoils/Blades and Wind Farm Layouts," Ph.D. Thesis, Washington University in Saint Louis, 2014.

[10] Abbott, I.H., and von Doenhoff, A.E., Theory of Wing Sections: Including a Summary of Airfoil Data, Dover, New York, NY, 1959.

[11] Castonguay, P., Liang, C., and Jameson, A., "Simulation of Transition Flow over Airfoils using the Spectral Difference Method," AIAA Paper 2010-4626, 40th AIAA Fluid Dynamics Conference and Exhibit, 28 June- 01 July 2010, Chicago, IL.

[12] ANSYS, 2012, Fluent Theory Guide, Canonburg, PA.

Vita

Binhe Song

Degrees M.S. Mechanical Engineering, Dec 2015
B.S. Mechanical Engineering, June 2011